Title
Systems Biology of Nutrient Homeostasis

Author
Margolin, Brian

Publication Date
2008-01-07

Peer reviewed|Thesis/dissertation

Systems Biology of Nutrient Homeostasis

by

Brian Margolin

DISSERTATION

Submitted in partial satisfaction of the requirements for the degree of

DOCTOR OF PHILOSOPHY

in

Biochemistry and Molecular Biology

in the

GRADUATE DIVISION

of the

UNIVERSITY OF CALIFORNIA, SAN FRANCISCO

UMI Number: 3289336

UMI Microform 3289336

ProQuest Information and Learning Company
300 North Zeeb Road
P.O. Box 1346
Ann Arbor, MI 48106-1346

Dedication

IN MEMORY OF MY GRANDMA, CLARA BERNSTEIN

WHO NEVER LOST FAITH IN ME

Abstract

Systems Biology of Nutrient Homeostasis

Brian Margolin

Organisms often live in variable environments with the amount of essential nutrients greatly varying. Nevertheless, it is imperative that the concentration of essential nutrients be kept relatively constant within the cell or organism. Upon starvation for the essential nutrient phosphate, *Saccharomyces cerevisiae* responds by upregulating a large class of genes that aids it in scavenging environmental phosphate as well as utilizing its internal phosphate stores. We found that the phosphate responsive signaling pathway responds in a bistable fashion. The bistable nature of the signaling pathway depends on the proper balance between multiple positive and negative feedback loops. Bistability in the signaling pathway may allow cells to anticipate and respond to changes in environmental phosphate.

Table of Contents

List of Tables

List of Figures

Chapter I: Introduction

The ability to process and act upon information is one of the defining characteristics of life. Cellular information processing typically involves interactions among numerous factors in complex pathways. Over the past 20 years or so, much progress has been made in identifying the many components and interactions of signaling pathways. Nevertheless, we are just beginning to understand how these components interact to form a system capable of interpreting signals (input) to generate the appropriate response (output). An understanding of cellular information processing depends upon the ability to determine quantitative relationships between input to a signaling system and output at various steps within that system.

Biological systems, like electronic systems, are composed of a relatively limited diversity of types of parts and interactions. Protein/ligand interactions and enzymatic catalysis follow precise thermodynamic and kinetic restraints. Nevertheless, biological signaling systems, like electronic systems, can "compute" a variety of precise and robust outputs for given inputs that cannot be predicted from knowledge of the individual components and interactions (Hartwell et al., 1999). For example, the *E. coli* chemotaxis system is sensitive to small changes in chemoattractant concentration over a very large dynamic range, yet maintains the ability to filter out random fluctuations of chemoattractant (Barkai and Leibler, 1997). On the other hand, the *X. laevis* progesterone-responsive MAP kinase

cascade responds to progesterone in a switch-like manner, i.e. the system is maximally responsive over an infinitesimally small progesterone concentration range; outside of that range, the system is insensitive to relatively large changes in progesterone concentration (Ferrell and Machleder, 1998).

For many signaling systems most, if not all, of the factors and interactions defining the system have been identified. Yet, it is becoming clear that signaling systems often exhibit complex behaviors that are not easily predictable from knowledge of the individual interactions. Although evidence of complex system behaviors is emerging, little is understood about how these complex properties are generated. Much of our understanding of signaling systems comes from experiments comparing system output at zero and saturating amounts of input. Additionally, many of these experiments have traditionally treated output as an all or none event. While these types of experiments have been very fruitful in identifying the components that comprise signaling pathways, they have not been able to provide much information about the function of systems as a whole.

System reactions do not happen in isolation; rather, they occur simultaneously and can affect one another's behaviors and rates. It is the interplay of the individual reactions of a signaling system that likely is responsible for generating complex system properties. Therefore, to understand how an integrated signaling system functions to produce these properties, it is important to study the system, not as a

set of isolated reactions, but rather, as a complete unit within the context of a living cell.

Chapter II: Characterization of the PHO Pathway

Introduction

Although much is known about the components of the PHO pathway and the genes that it activates, detailed quantitative knowledge about the expression of individual PHO-induced genes is limited to two well characterized genes, *PHO5* and *PHO84* (Springer et al., 2003; Thomas and O'Shea, 2005). Although both *PHO5* and *PHO84* are induced under phosphate starvation conditions, their expression profiles are remarkably different. At intermediate levels of phosphate starvation *PHO84* is induced to approximately 50% of its maximal level, i.e. its level of expression under complete phosphate starvation. In contrast, *PHO5* is induced to a very low level (approximately 5% of maximal induction) in intermediate phosphate conditions and is only significantly induced when environmental phosphate levels drop to near zero (Springer et al., 2003).

Furthermore, a more subtle difference between *PHO5* and *PHO84* expression is apparent. When expression is measured at the single-cell level, *PHO84* is induced in a bimodal, i.e. all or none fashion, in response to phosphate starvation (Thomas and O'Shea, 2005). Cells either express *PHO84* at near maximum levels, or at near basal levels. Few, if any, cells express *PHO84* at intermediate levels. On the other hand, *PHO5* appears to be expressed in a graded manner. At low levels of pathway

activation, *PHO5* is expressed at a low level, at intermediate levels of pathway activation, *PHO5* is expressed at an intermediate level and at high levels of pathway activation *PHO5* is expressed at high levels*.

It is easy to imagine that the quantitative transcriptional profiles of various PHO-induced genes reflect the functional necessity of their gene products in various environmental conditions. For example, it would be beneficial to express Pho84, a high affinity phosphate transporter, in intermediate phosphate conditions to allow the cell to continue to import phosphate even though environmental phosphate concentrations are lower. On the other hand, it would only be necessary to express Pho5, a secreted acid phosphatase, when environmental phosphate concentrations drop to asymptotically low levels to enable the cell to scavenge organically bound phosphate from its environment. Nevertheless, the mechanisms by which the PHO pathway achieves this promoter by promoter optimization are not well understood.

---

* Because *PHO5* is not significantly induced until environmental phosphate drops to extremely low levels, it is technically difficult to quantitatively measure its level of transcription in response to varying phosphate concentrations. Therefore, the graded response was measured by chemically inhibiting the key PHO pathway kinase, Pho85 (Thomas, M.R., Unpublished Data).

It is surprising and difficult to understand how *PHO5* and *PHO84* are expressed in such different manners. Both promoters, like all other known PHO promoters, are induced under conditions of phosphate starvation solely due to the relocalization and activation of the transcription factor Pho4. Yet when cells are grown under intermediate phosphate conditions, although Pho4 is active and localized to the nucleus, only *PHO84* is significantly activated. Additionally, it is difficult to understand how the activation of a single transcription factor can lead to transcriptional induction in both a graded and ultra-sensitive fashion depending on the promoter that it is activating (Springer et al., 2003).

It is possible that each promoter's distinctive response to PHO pathway activation is due solely to specific characteristics of each promoter, independent of the PHO pathway. Alternatively, specific features and behaviors of the PHO pathway itself, in collusion with the various PHO promoters, may be required to generate the detailed quantitative difference between *PHO5* and *PHO84* promoter activation. Furthermore, it is unclear if the difference in activation thresholds between *PHO5* and *PHO84* is coupled to the difference in apparent Hill coefficient of their responses. For example, we could imagine the existence of a PHO promoter that is induced in intermediate phosphate conditions (similar to *PHO84*) and in a graded manner (similar to *PHO5*), yet it is unclear if a promoter like this does or could exist. Likewise, could a promoter that is only induced at near-zero phosphate conditions

(similar to *PHO5*) yet in a bimodal fashion (similar to *PHO84*) exist? It may be that these two quantitative "phenotypes" are intricately linked and therefore inseparable, foregoing the possible existence of either of these putative promoter types. Because we know little about the quantitative response profiles of other PHO promoters, it is difficult to even begin to address questions such as these.

Microarray experiments have identified a set of approximately 22 promoters that are activated by Pho4 in response to phosphate starvation (Carroll et al., 2001; Ogawa et al., 2000). Although it is clear that the *PHO5* and *PHO84* promoters show distinct quantitative differences in their response to PHO pathway activation, it was not known how other PHO promoters quantitatively responded to PHO pathway activation. Although microarray analysis had been beneficial in identifying genes that are induced by Pho4 when starved for phosphate, it is not possible to further characterize the quantitative responses of these promoters using microarray technology. This is for two reasons. First, as a population average measurement, microarray analysis (or any bulk RNA measurement technique, for that matter) is not capable of discerning ultrasensitive from graded transcriptional responses.

Results

Survey of transcriptional responses in the PHO pathway. To gain an understanding into how each of the approximately 22 PHO-regulated genes responds to activation of the Pho pathway, I built a library of yeast strains that allowed me to quantitatively analyze gene expression in single cells from each of the PHO-regulated genes. In each library strain, I replaced the coding region of one of the PHO-regulated genes with a GFP reporter so that GFP was produced by induction of that gene's promoter rather than its own gene product. I then analyzed each gene's response to a range of phosphate conditions in single cells. To prevent possible feedback effects due to deletion of PHO genes, library strains were diploid, with only one copy of each gene replaced by GFP. Therefore, each strain was heterozygous for the gene that was being analyzed.

Eleven cultures of each library strain were grown at low cell density for 3 hours in SD media supplemented with KH_2PO_4 to achieve phosphate concentrations ranging from zero to 10mM. Although cell growth may have begun to deplete media phosphate concentrations by the end of the experiment, the time period of growth was short enough that GFP accumulation at the time of analysis likely reflected only

initial transcriptional induction*. Expression was analyzed by flow cytometry so that measurements were done at the level of single cells (Table 2.1).

Two classes of PHO gene thresholds. When analyzed, all of the PHO promoters tested fell into two broad classes in terms of the environmental phosphate concentration at which they were activated (Figure 2.1). One group of promoters was not significantly induced until cells were almost completely starved for phosphate. A second group of promoters was activated at intermediate levels of phosphate starvation. These two promoter classes correspond to the originally observed difference between *PHO5* (heavy red line) and *PHO84* (heavy green line) expression profiles.

The *PHO5* promoter is arguably one of the most well characterized eukaryotic promoters. It contains two binding sites for the bHLH transcription factor Pho4, one site, which matches the Pho4 consensus hexameric binding sequence, and binds

* These initial experiments were performed before it was clear to us how quickly phosphate was depleted by cultures. All subsequent experiments were performed such that we could be certain that phosphate concentrations in the media were not depleted before the end of the experiment. The data generated by these experiments has since been verified by Felix Lam (unpublished results) for some of the library strains.

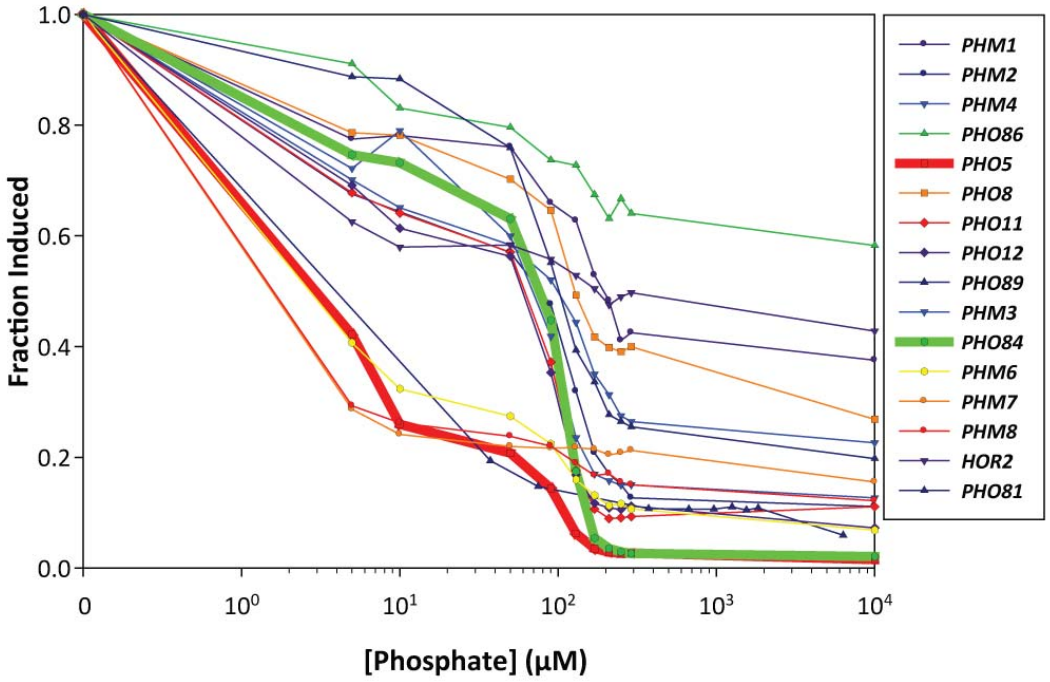

Figure 2.1: Flow Cytometric Analysis of PHO Promoters.

Table 2. 1

[Phosphate] (µM):	*0*	*5*	*10*	*38*	*50*	*75*	*90*	*130*	*170*	*210*	*250*	*290*
HOR2	1.0	0.35	0.27		0.27		0.23	0.18	0.13	0.08	0.11	0.12
PHM1	1.0	0.64	0.65		0.62		0.45	0.40	0.25	0.17	0.06	0.08
PHM2	1.0	0.64	0.60		0.52		0.41	0.23	0.11	0.07	0.04	0.02
PHM3	1.0	0.68	0.76		0.54		0.33	0.12	0.05	0.04	0.03	0.03
PHM4	1.0	0.61	0.55		0.46		0.38	0.28	0.16	0.11	0.06	0.05
PHM6	1.0	0.36	0.27		0.22		0.17	0.10	0.07	0.05	0.05	0.04
PHM7	1.0	0.16	0.10		0.08		0.07	0.07	0.07	0.06	0.06	0.07
PHM8	1.0	0.20	0.16		0.13		0.11	0.08	0.05	0.06	0.04	0.03
PHO5	1.0	0.41	0.25		0.20		0.13	0.05	0.02	0.01	0.01	0.01
PHO8	1.0	0.71	0.70		0.59		0.52	0.31	0.20	0.18	0.17	0.18
PHO11	1.0	0.64	0.60		0.52		0.29	0.07	0.00	-0.02	-0.02	-0.02
PHO12	1.0	0.67	0.58		0.53		0.30	0.10	0.05	0.04	0.04	0.04
PHO81	1.0	0.86	0.85		0.70		0.44	0.24	0.17	0.10	0.08	0.07
PHO84	1.0	0.74	0.73		0.62		0.44	0.16	0.03	0.01	0.01	0.01
PHO86	1.0	0.79	0.59		0.51		0.37	0.35	0.22	0.12	0.20	0.14
PHO89	1.0	0.20		0.14		0.09						

with relatively high affinity and a second site, which differs from the consensus binding site by a single base and binds with lower affinity (Maerkl and Quake, 2007; Vogel et al., 1989). The *PHO84* promoter, on the other hand, has four Pho4 binding sites, two of them high affinity sites and two of them low affinity (Bun-Ya et al., 1991). I initially thought that the number and/or affinity of Pho4 binding sites in a given promoter would determine whether it responded at low or intermediate phosphate. Nevertheless, careful analysis of the promoter sequences showed no correlation between the number and/or affinity of Pho4 binding sites in a given promoter and its phosphate response profile.

PHO84 is the only PHO gene that is obviously bimodally expressed. Although Pho84 is expressed in a bimodal fashion, most of the other PHO-regulated genes appeared to respond in a graded fashion (Figure 2.2)[*]. At the time these experiments were

[*] Although we now know that *SPL2* is also expressed in a bimodal fashion in response to phosphate starvation, the initial screen showed no evidence of *SPL2* induction upon phosphate starvation. Subsequent analysis and experiments showed that *SPL2* was incorrectly annotated in the literature and The *Saccharomyces* Genome Database. What was reported as the initiating codon, was in fact upstream of the TATA box. Therefore, fluorescent reporters driven by the incorrectly annotated promoter were not induced by phosphate starvation. Using bioinformatic techniques, I have

performed, only a relatively inefficient GFP variant was available. Therefore, genes that are not expressed at high levels may have appeared to be expressed in a graded fashion due to an inability to separate high vs. low expression fluorescence. Nevertheless, this suggested a key role for *PHO84* in the phosphate pathway and led me to further pursue studies of this phenomenon.

Systems analysis of PHO84 expression. My initial studies of Pho84 expression were done in a diploid strain that was heterozygous for *PHO84*. To better explore the phenomenon I built a reporter strain in which I replaced the *PHO84* ORF with GFP. Additionally, I placed a functional copy of *PHO84* at an ectopic locus to allow for proper Pho84-dependent pathway feedback. Initial experiments with this strain showed that *PHO84* expression was indeed bimodal. Additionally, the strain exhibited strong hysteresis. Cells that were grown in low phosphate, and therefore expressing *PHO84*, continued to express *PHO84* even after the addition of high phosphate to the media. This phenotype was verified by cell sorting, plating and microscopy experiments (data not shown).

---

since identified the correct initiating codon, which has allowed me to accurately measure *SPL2* promoter expression levels (see appendix).

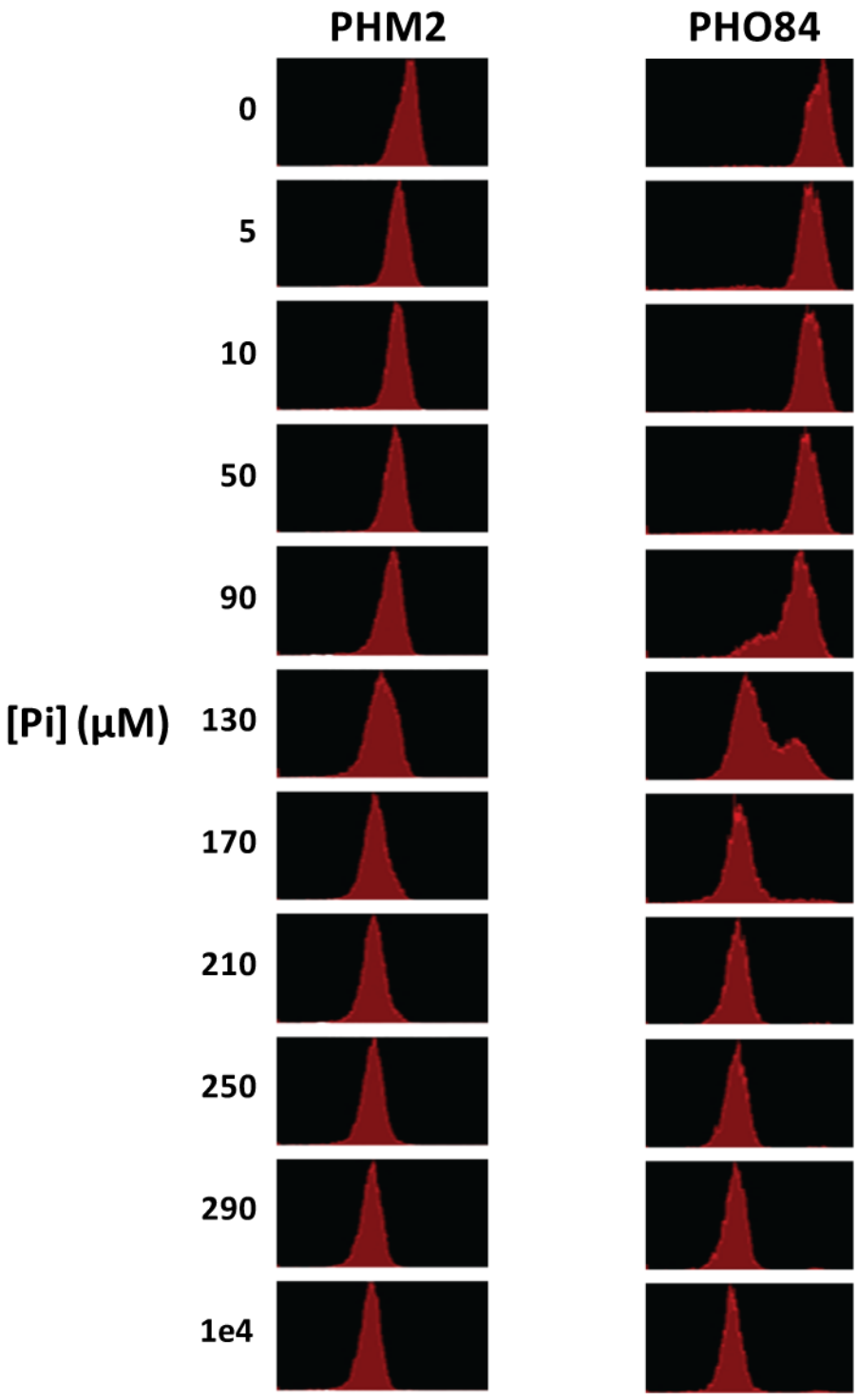

Figure 2.2: Representative flow cytometry histograms.

Although these data indicated a very strong level of hysteresis, previous experiments measuring *PHO84* mRNA levels in wild-type strains (which are albeit population measurements) did not indicate these high levels of hysteresis. In fact, the strong hysteresis of my reporter strain was reminiscent of the constitutive activation of the PHO pathway in *pho84Δ* strains.

It therefore seemed plausible that a lower level of *PHO84* expression in the reporter strain, due to the placement of the functional copy of *PHO84* at an ectopic locus, may have been responsible for the strong hysteresis that was observed. To test this I generated new reporter strains containing functional copies of *PHO84* at its native locus and *PHO84*-promoted fluorescent reporters at various ectopic loci. Following generation of these strains, I measured the transcriptional response of *PHO84* in response to varying environmental phosphate concentrations. The maximal level of GFP was in fact lower in these strains, consistent with the hypothesis that the *PHO84* promoter is, in fact, less transcriptionally competent at the tested ectopic loci (Data not shown). These new reporter strains were used for all subsequent experiments.

Theoretical sources of bimodality. Bimodality in a signaling system can arise from at least two distinct mechanisms. A signaling system is said to be ultra-sensitive if, around some threshold point, a small change in input to the signaling pathway leads to a relatively large change in output of the signaling pathway (see Figure 2.3).

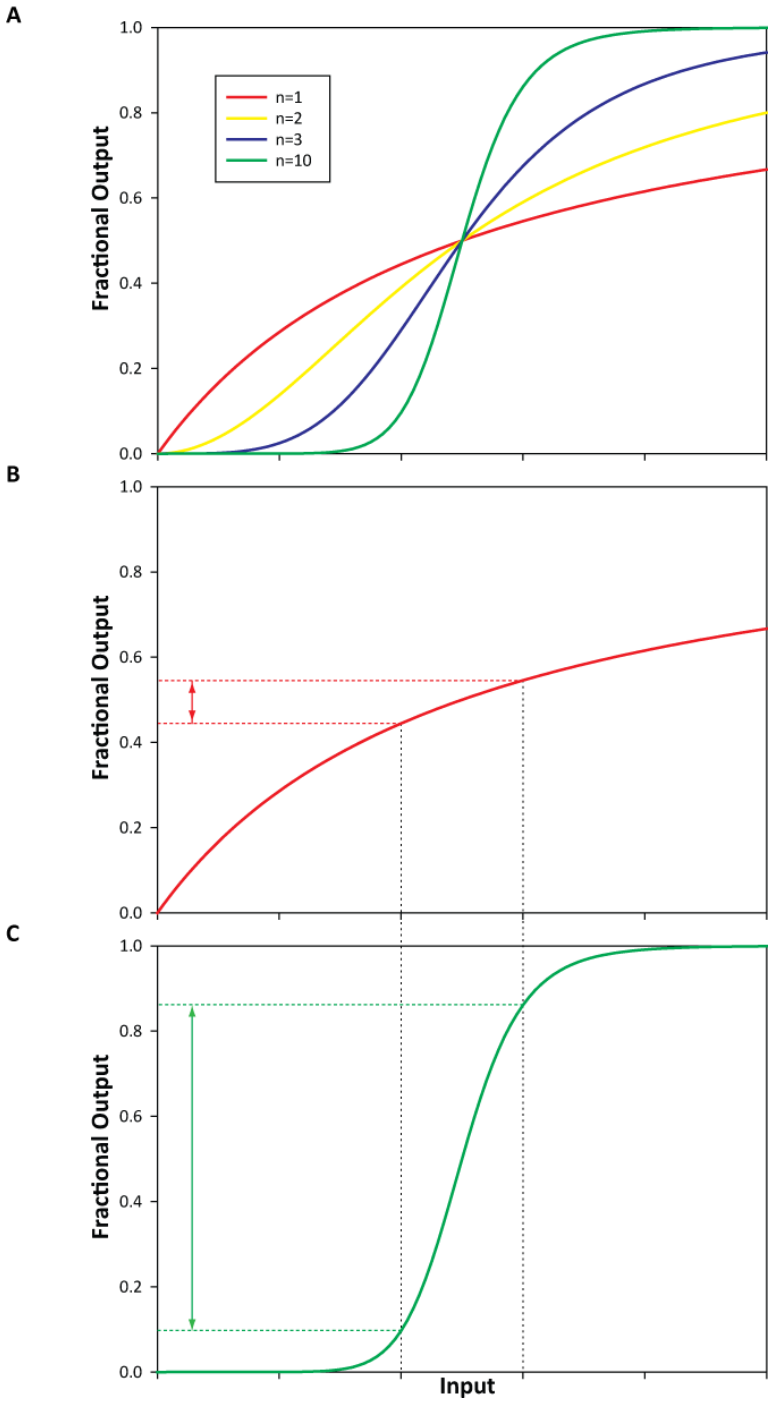

Figure 2.3: Bimodality as a consequence of ultra-sensitivity and noise.

Although ultra-sensitivity can arise from numerous mechanisms, all ultrasensitive systems exhibit this behavior.

When we talk about cells in a clonal population, we tend to think about these cells as being fundamentally identical to one another. Yet, this is not the case. Even if we forgo the fact that genomes are constantly acquiring, and often repairing, mutations, it is clear that genotypically identical cells can be phenotypically diverse. This is most clear for multi-cellular organisms where a given organism can be made up of multitudes of diverse cell types, even though each of these types is genotypically identical. The case is less clear for single-celled organisms, where at least superficially, all cells of a given population seem to be identical. Recent studies have highlighted widespread variability in protein expression throughout the yeast proteome (Bar-Even et al., 2006; Newman et al., 2006). Whether this cell to cell variability is just a consequence of a stochastic universe, having little effect on an organism's fitness, or is actually functionally relevant and evolutionarily selected for is unknown. Nevertheless, we are just beginning to understand the potential consequences stochastic variability can have on populations of cells.

Were biological systems "perfect", we would expect that for a given population of cells, all cells would be identical. Therefore, the measured output of a given signaling pathway should be invariant from cell to cell and should be equal to the population mean. Nevertheless, as discussed above, even within a single culture of

yeast cells, wide cell to cell variability in the levels of most proteins exists. Variation in the levels of proteins components of a signaling pathway can easily affect the system's transfer function. Therefore, when measuring signaling pathways at the level of single cells, a range of outputs bounding the population average is typically detected for any given input (Maheshri and O'Shea, 2007).

For signaling systems that are activated in a graded fashion, this leads to a cell-cell lognormal distribution of signaling outputs (Bar-Even et al., 2006; Newman et al., 2006). On the other hand, for signaling systems that exhibit ultra-sensitive behavior, the ON/OFF nature of the pathway can act to both reduce as well as increase cell-cell variability relative to that obtained from a graded signaling pathway. The sigmoidal nature of an ultra-sensitive response (see Figure 2.3-C) leads to regions of decreased as well as increased sensitivity to input conditions relative to a graded response. Around the threshold value, the slope of an ultra-sensitive response is large relative to a graded response. Therefore, small perturbations in either input conditions or components of the signaling pathway lead to relatively large changes in output values, e.g. green arrow in Figure 2.3-C, relative to the same region of a graded signaling pathway, e.g. red arrow in Figure 2.3-B. On the other hand, at input values farther from the threshold value, the slope of an ultra-sensitive response is small relative to a graded response. At these input values, rather large pathway perturbations lead to relatively small changes in

output values. The overall effect of ultra-sensitivity then, is to compress the region of noise susceptibility to a small region flanking the threshold value. At input values flanking a system's threshold value therefore, small stochastic differences between cells leads to large output differences that approach two distinct cell populations as the system's Hill coefficient gets large enough. It is important to note that variation of a signaling system's Hill coefficient has no effect on the mean population response to system input, but has a drastic effect on cell-cell variability in system response.

Characterization of PHO84 bimodality. To characterize the transcriptional response of *PHO84* to decreasing amounts of environmental phosphate, I built a haploid yeast strain bearing the *PHO84* promoter driving the expression of a yeast codon optimized variant of enhanced GFP (Cormack et al., 1996) at the yeast *URA3* locus (EY1995). The native copy of *PHO84* remained unperturbed in this strain. To measure *PHO84* expression levels EY1995 was inoculated into SD media containing varying concentrations of K_2HPO_4 and grown for 18 hours followed by fluorescence analysis by flow cytometry. Time course experiments were used to determine that an 18 hour time point was significantly past the time required to reach steady-state GFP levels. Phosphate is used at a high rate by yeast cultures and the concentration of phosphate in media is therefore readily depleted by growing cultures. To ensure that phosphate concentrations in the media were not perturbed during the course of all phosphate titration experiments, cell densities were kept below $5x10^4$ cells/ ml.

Initial experiments determined appropriate cell densities by establishing cell densities that did not significantly perturb phosphate concentrations in SD media through 18 hours of growth.

As expected, at high external phosphate concentrations, the PHO pathway is inactive and consequently GFP fluorescence levels were low (Figure 2.4). At low external phosphate levels the PHO pathway is active and consequently GFP fluorescence levels were high. At intermediate phosphate levels, though, GFP fluorescence was not at an intermediate level. Rather, the population of cells in the culture split into two distinct populations, one showing low levels of GFP fluorescence and one showing high levels (Thomas and O'Shea, 2005). Through this intermediate range, as the concentration of phosphate in the media is decreased, the fluorescence level of these two populations did not change. Rather, the fraction of cells existing in either of these two populations did. At the phosphate concentration was lowered, a higher proportion of cells populated the high fluorescence fraction until finally all cells were represented in the high fluorescence population.

PHO84 expression is bistable. The appearance of bimodality in the response of a signaling system indicates that the signal response is, in some manner, ultra-sensitive. On the other hand, a bimodal response does not indicate the source of the ultra-sensitivity. Bimodality can arise from one of, at least, two possible mechanisms. Traditionally, we think of ultra-sensitivity as arising from classical

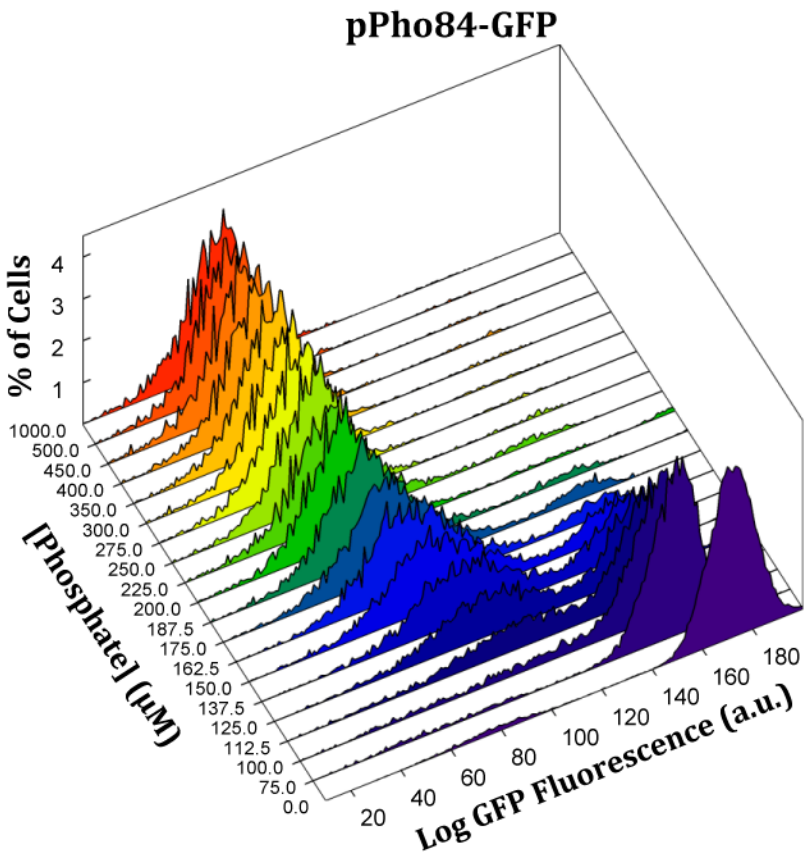

Figure 2.4: Bimodal Expression from PHO84 Promoter.

biochemical cooperativity at the level of signaling. This leads to a Hill coefficient greater than one for the system and increases the sensitivity of a system to its initial input. As the level of cooperativity within a signaling system is increased, the relative variance of output states is increased at points around the input threshold. As the level of cooperativity is further increased, the variance of output states is increased until finally most cells lie at opposite ends of the output distribution, i.e. the system appears bimodal (see Figure 2.3-C). When thinking of a single biochemical reaction, it is difficult to imagine a Hill coefficient high enough to generate bimodality from that reaction. In the case of a signaling pathway, though, it is the net apparent Hill coefficient of the pathway that is relevant. For a signaling network, an apparent high level of cooperativity may be composed of many smaller Hill coefficients pertaining to individual reactions within the pathway.

Bistability is another mechanism that can generate bimodality in a signaling pathway (for a more theoretical discussion of bistability see Chapter 3). A bistable system is one in which, for at least some range of input values, two stable steady states exist. For a system to exhibit bistability, some level of positive feedback must exist in the system. A system that exhibits a bimodal signaling response may be bistable. On the other hand, it may just exhibit a high level of cooperativity. The presence of two stable steady states for a given input value is a clear indication of the presence of bistability in a signaling system. The population of a given stable

steady state in a bistable system is determined by the history of the system, i.e. the starting conditions and trajectory the system takes in reaching the stable steady state (hysteresis). Therefore, to determine if a signaling system is bistable, a comparison of the quantitative analyses of the system response when beginning the analysis from either an induced or uninduced state is useful.

To determine if *PHO84* expression is bistable, I built a haploid yeast strain bearing the *PHO84* promoter driving the expression of a yeast codon optimized variant of cerulean CFP (Kremers et al., 2006; Sheff and Thorn, 2004) at the yeast *HIS3* locus (strain EY2415). Additionally, so that the PHO pathway was being measured using more than one PHO-induced promoter, the strain was built with the *SPL2* promoter driving the expression of a yeast codon optimized variant of citrine YFP (Griesbeck et al., 2001; Sheff and Thorn, 2004) integrated at yeast *URA3* locus. The native copies of both *PHO84* and *SPL2* remained unperturbed in this strain. To analyze the PHO pathway for bistability, EY2415 was inoculated into SD media containing either 10mM (from high) or 100 μM (from low) K_2HPO_4 and grown for 4 hours. Following these initial incubations, these cultures were each inoculated into SD media containing varying concentrations of K_2HPO_4 and grown for 18 hours followed by fluorescence analysis by flow cytometry (Figure 2.5).

A bimodal signaling system that is not bistable shows the same induction profile, independent of the history of the system. On the other hand, a bistable system is

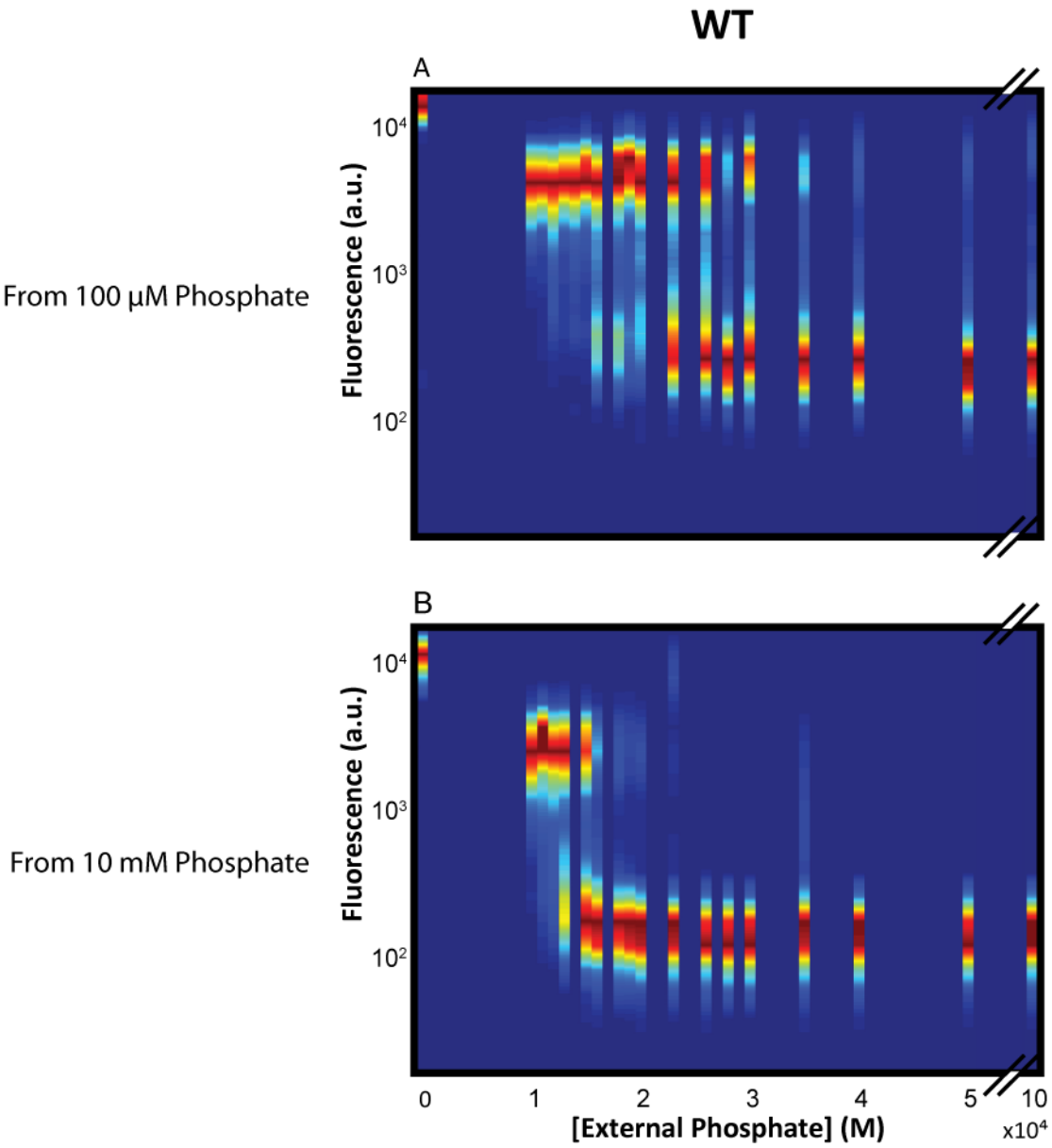

Figure 2.5: Bistable expression from the SPL2 Promoter.

expected to show a different induction profile depending on the starting state of the system. As can be seen in Figure 2.5, there is a clear difference in the induction profiles depending on the starting condition at the beginning of the experiment. The PHO pathway, as evidenced by expression of *SPL2*, is completely off by approximately 175 μM phosphate when starting from an uninduced state (panel B). On the other hand, when the phosphate titrations were begun with induced cultures, some cells remain induced even when the phosphate concentration is as high as 400 μM. This indicates that the PHO pathway is indeed bistable.

Sources of bistability. Bistability in biological systems can arise from a number of mechanisms, all of which require positive feedback at some level. One mechanism is the combination of a positive feedback loop with a non-linear system response in the signaling pathway. Therefore, I was interested in determing possible sources of positive feedback in the pathway. Two members of the O'Shea Lab, Jonathan Raser and Dennis Wykoff, hypothesized that positive feedback in the Pho pathway could arise due to down-regulation of low affinity phosphate transporters upon phosphate starvation (Figure 2.6). Although the low affinity phosphate transporters are not transcriptionally regulated by phosphate, a number of esoteric pieces of evidence suggested that the activity of these low affinity transporters was inhibited during phosphate starvation (Wykoff et al., 2007).

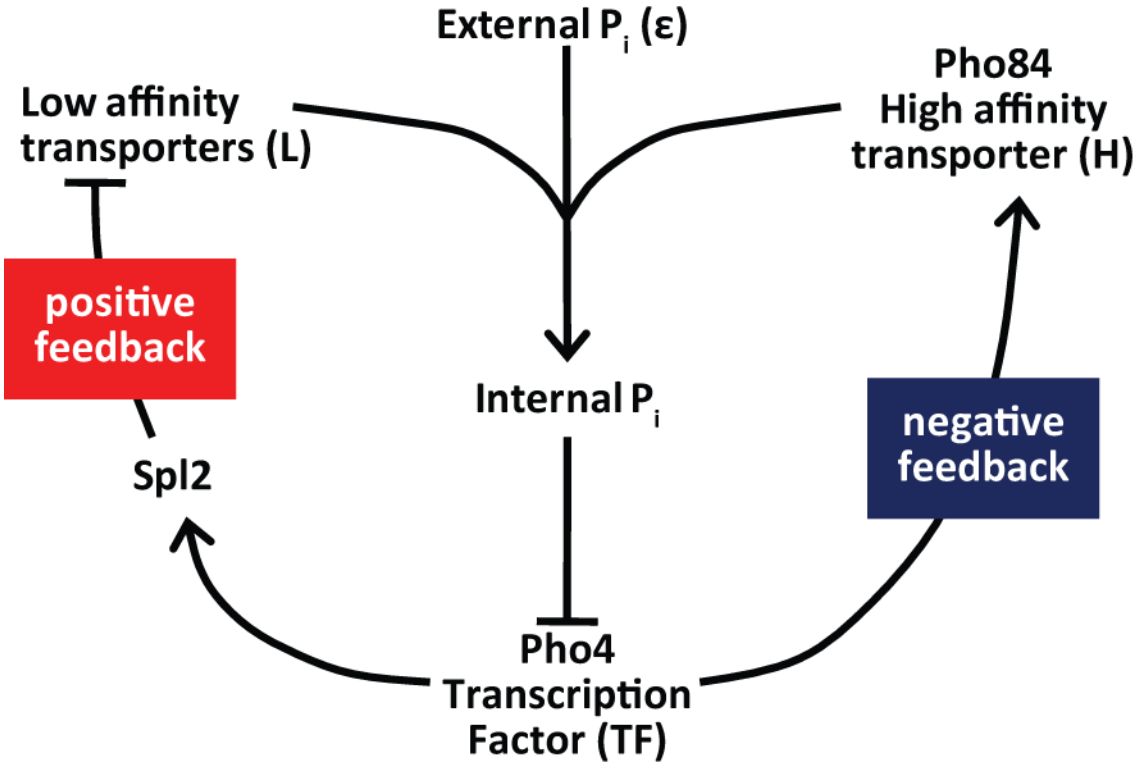

Figure 2.6: Model for Bistability in the PHO Pathway.

Kinetics of Phosphate Uptake in pho84 Deletion Strains. Although indirect evidence suggested that the activity of low affinity phosphate transporters was down-regulated in response to phosphate starvation, little direct evidence existed. To directly test this prediction of the model, I measured phosphate uptake kinetics in *pho84* deletion strains.

I measured the kinetics of phosphate uptake in a number of yeast strains and conditions. The tested strains included a pho84Δ strain (EY0105) and a pho84Δ pho4Δ strain (EY0329). Therefore, the measured phosphate uptake parameters were due solely to low affinity phosphate transporters. Yeast strains were grown in either high or low phosphate media, washed and then resuspended in media with a range of phosphate concentrations, each spiked with a small amount of ^{32}Pi. Following various incubation times, each culture was filtered and washed. The amount of phosphate taken up by the cells was then measured by scintillation counting.

In the *pho84*Δ strain grown in high phosphate conditions, phosphate transport is primarily low-affinity ($K_m \sim 200$ μM phosphate) (Wykoff and O'Shea, 2001). When starved for phosphate, cells lacking Pho84 lose almost all phosphate transport, indicating that low-affinity transport is down-regulated in response to phosphate availability (Figure 2.7). Inactivation of the downstream transcription factor Pho4 prevents this down-regulation; the *pho84*Δ *pho4*Δ strain displays little change in

phosphate uptake in response to phosphate starvation (Figure 2.7). Therefore, a functional PHO pathway is required for down-regulation of low-affinity phosphate transport in response to phosphate limitation.

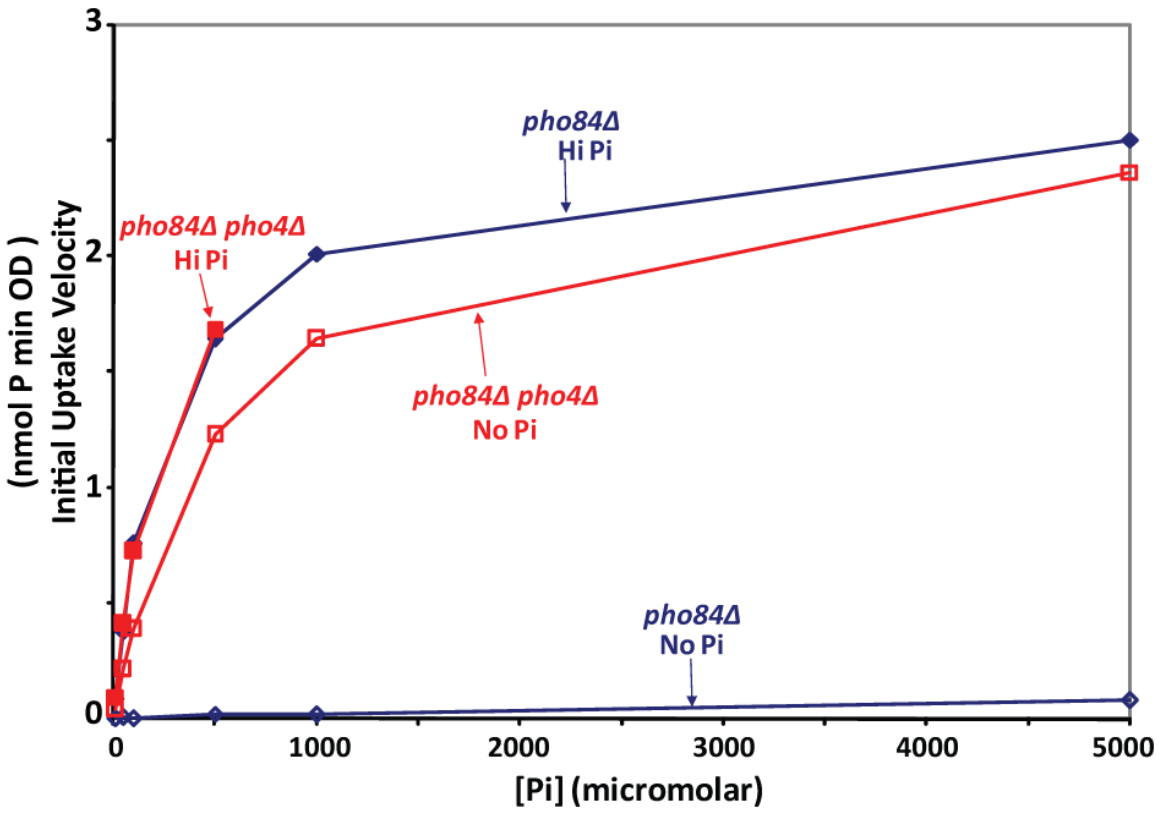

Figure 2.7: **Kinetics of Phosphate Uptake in *pho84* Deletion Strains.**

Figure Legends

Figure 2.1: Flow Cytometric Analysis of PHO Promoters. Diploid heterozygous strains were grown for three hours in synthetic media supplemented with K_2HPO_4 at concentrations ranging from zero to 10 mM. Cells were inoculated at low numbers to prevent phosphate depletion due to cell usage. For each strain, the median fluorescence values were normalized to the strain's maximum fluorescence level, i.e. in no phosphate media and plotted versus the phosphate concentration of the media on a log axis. *PHO5* and *PHO84* are indicated with heavy red and green lines, respectively.

Figure 2.2: Representative flow cytometry histograms. Diploid heterozygous strains were grown for three hours in synthetic media supplemented with K_2HPO_4 at concentrations ranging from zero to 10 mM. Cells were inoculated at 1×10^4 / ml to prevent phosphate depletion due to cell usage. Histograms showing relative number of cells at median fluorescence values are shown for *PHM2* and *PHO84* strains.

Figure 2.3: Bimodality as a consequence of ultra-sensitivity and noise. For the shown equation fraction of maximum output is plotted vs. input using values of 1 for both

k_m and V_{max}. **A.** Response curves using Hill coefficients (n_H) of 1, 2, 3, 10 for red, yellow, blue and green curves respectively. **B and C.** Response curves with Hill coefficients of 1 (B) and 10 (C). Dashed black lines indicate range of input signal noise. Dashed red and green lines indicate ranges of output values for given input noise with Hill coefficients of 1 and 10 respectively.

Figure 2.4: Bimodal Expression from PHO84 Promoter. Strain EY1995 was grown for 18 hours in synthetic media supplemented with K_2HPO_4 at concentrations ranging from zero to 1 mM. Cells were inoculated at low density to prevent phosphate depletion due to cell usage. For each culture, histograms showing the percent of cells versus median fluorescence value are shown for all phosphate concentrations tested.

Figure 2.5: Bistable expression from the SPL2 Promoter. Strain EY2415, (*pPHO84*-Cerulean *pSPL2*-Citrine) was grown overnight to mid-log phase (OD_{600} = 0.2) in synthetic media supplemented with 10 mM K_2HPO_4. Cultures were then washed and resuspended in fresh media containing either 100 μM or 10mM K_2HPO_4, grown for 4 hours and then diluted into fresh synthetic media supplemented with K_2HPO_4 at concentrations ranging from zero to 1 mM. To prevent phosphate

depletion, cells were inoculated at densities so that after 18 hours of growth there were approximately 5x 10^4 cells/ml. For each culture, density maps display the fraction of cells showing the indicated median YFP fluorescence value for all phosphate concentrations tested.

Figure 2.6: Model for Bistability in the PHO Pathway.

Figure 2.7: Kinetics of Phosphate Uptake in pho84 Deletion Strains. Phosphate uptake kinetics were measured from *pho84Δ* strains grown in either 10 mM (blue lines) or no phosphate media (red lines). Phosphate transport through low affinity transporters was inhibited by growth in no phosphate media in *PHO4* (filled markers), but not *pho4Δ* (unfilled markers) strains. *pho84Δ* strains were grown overnight in synthetic media plus 10 mM K_2HPO_4 to mid-log phase. Cultures were then washed and resuspended in synthetic media with or without 10mM K2HPO4 for 5 hours. Cells were then washed in synthetic no phosphate media, resuspended in synthetic media supplemented with various amounts of K_2HPO_4, each spiked with a small amount of $^{32}P_i$. Cultures were grown for 2 minutes and then harvested on ice to stop growth and amount of $^{32}P_i$ incorporated was measured by scintillation counting after filtration.

Chapter III: A Mathematical Model of the PHO Pathway

Introduction

Early investigations of the PHO pathway gave a lot of insight into the specific components and mechanisms involved in signal transduction in response to phosphate starvation. Additionally, detail about the genes that are affected by PHO pathway induction was uncovered. While continued investigation of the PHO pathway has uncovered many of its details, it has also revealed more complex behaviors that we are just beginning to understand. The PHO pathway is bistable and this bistability leads to ultra-sensitivity, yet the mechanism and function of these behaviors is still unknown. It seems intuitive that the presence of positive feedback in a signaling pathway can lead to hysteresis and/or switch-like behavior. Nevertheless, it is clear that the presence of positive feedback alone is not sufficient to generate these behaviors (see (Angeli et al., 2004)). Furthermore, the specific features, in addition to positive feedback, required to generate these behaviors depends on the system in question.

As an aid to understanding the origin, features and function of bistability in the PHO pathway, we decided to mathematically model the system as we understood it. In this aspect of the project, I owe much gratitude to Narendra Maheshri for aid in modeling and numerous late night conversations regarding the esoterica of the PHO pathway. Specifically we were interested in determining if positive feedback due to

down-regulation of low affinity phosphate transporters could be involved in the generation of bistability.

Results

A mathematical model of the PHO pathway. We understand many, but not all, details about the functioning of the PHO pathway. Nevertheless, the features of the pathway relevant to a steady-state understanding can be encapsulated in a series of three differential equations that describe the time dependent concentrations of low affinity transporters (L), high affinity transporters (H) and phosphate inside the cell (P).

$$\frac{\partial H}{\partial t} = \frac{\beta_H}{\left(\frac{P}{T_H}\right)^{n_h} + 1} - H\gamma \tag{3.1}$$

$$\frac{\partial L}{\partial t} = \frac{\beta_L}{\left(\frac{T_L}{P}\right)^{nl} + 1} - L\gamma \tag{3.2}$$

$$\frac{\partial P}{\partial t} = \frac{H\varepsilon V_H}{\varepsilon + k_H} + \frac{L\varepsilon V_L}{\varepsilon + k_l} - P\gamma \tag{3.3}$$

The concentrations of L and H depend on:

- the maximal production rates of L and H (β_L and β_H)
- the growth rate (γ)

- the threshold concentrations of internal phosphate at which the production of L and H are effected (T_L and T_H)
- the Hill coefficient of these responses (n_L and n_H)
- their own concentrations

The concentration of P depends on:

- The concentrations of L and H
- The external phosphate concentration (ε)
- The V_{max} of low and high affinity transporters (V_L and V_H)
- The k_m of low and high affinity transporters (k_L and k_H)

Parameter optimization. A number of the parameters used in the model have been experimentally measured by me or other members of the O'Shea Lab. Among the measured parameters are the V_{max} and K_m for both low and high affinity transporters(Wykoff and O'Shea, 2001) and growth rates at different phosphate concentrations (data not shown). Additionally, although we do not know the maximal production rates of the low and high affinity transporters (β_L and β_H) as

absolute values, we can solve for them in terms of maximal levels of L and H*. Other parameters in the model are less well understood, such as thresholds for induction of *PHO84* (T_H) and *SPL2* (T_L) synthesis as well as the Hill coefficients for these processes (n_H and n_L respectively) (Table 3.1).

By systematically varying model parameters, it is possible to fit the four unmeasured parameters to experimental data, i.e. the level of Pho84 as a function of external phosphate. By doing this we have estimated the values of T_H, T_L, n_H and n_L to be 0.06, 0.11, 6 and 6 respectively (Table 3.1).

Determination of system fixed points. As a non-linear dynamical system, there is no closed form solution for this system of equations. Nevertheless, we can learn a lot about the system both through numerical simulations of its time-dependent behavior as well as by analysis of its steady-state behavior. By definition, at steady state, the concentrations of H, L and P are constant. Therefore, we can solve for their concentrations at steady state by setting the three differential equations equal

---

* For example, in the $\lim_{P\to\infty}$ of equation 3.2, $\frac{T_L}{P} \to 0$ and therefore $\beta_L = L\gamma$. Since L is maximal in high phosphate, we can express L as a fraction of max L, i.e. 1 and therefore $\beta_L = \gamma$.

to zero, solving Equations (3.1) and (3.2) for the steady state concentrations of L and H in terms of P and plugging these equations into equation (3.3), yielding:

$$\frac{\partial P}{\partial t} = \underbrace{\frac{\varepsilon\left(\frac{V_H\beta_H}{\left(\varepsilon+k_H\right)\left(\left(\frac{P}{T_H}\right)^{n_H}+1\right)}+\frac{V_L\beta_L}{\left(\varepsilon+k_L\right)\left(\left(\frac{T_L}{P}\right)^{n_L}+1\right)}\right)}{\gamma}}_{\text{Uptake}} \underbrace{-P\gamma}_{\text{Dilution}} = 0 \qquad (3.4)$$

Equation (3.4) describes the time dependent concentration of phosphate inside the cell and is composed of two terms; one describing the phosphate import rate and the other the phosphate dilution rate. By definition, at steady state these two terms must be equal. We can calculate the number and position of fixed points, i.e. steady states, for the system by evaluating equation 3.4 at specific external phosphate concentrations. Additionally, we can visualize the fixed points by plotting the two rates from equation 3.4 as a function of [internal phosphate] and noting the points at which the two rates are intersect, i.e. points at which they are equal (Figure 3.1). As can be seen in Figure 3.1, although only one steady state exists for cultures grown in either high or low phosphate media, three steady states exist for cultures grown in intermediate phosphate (circles).

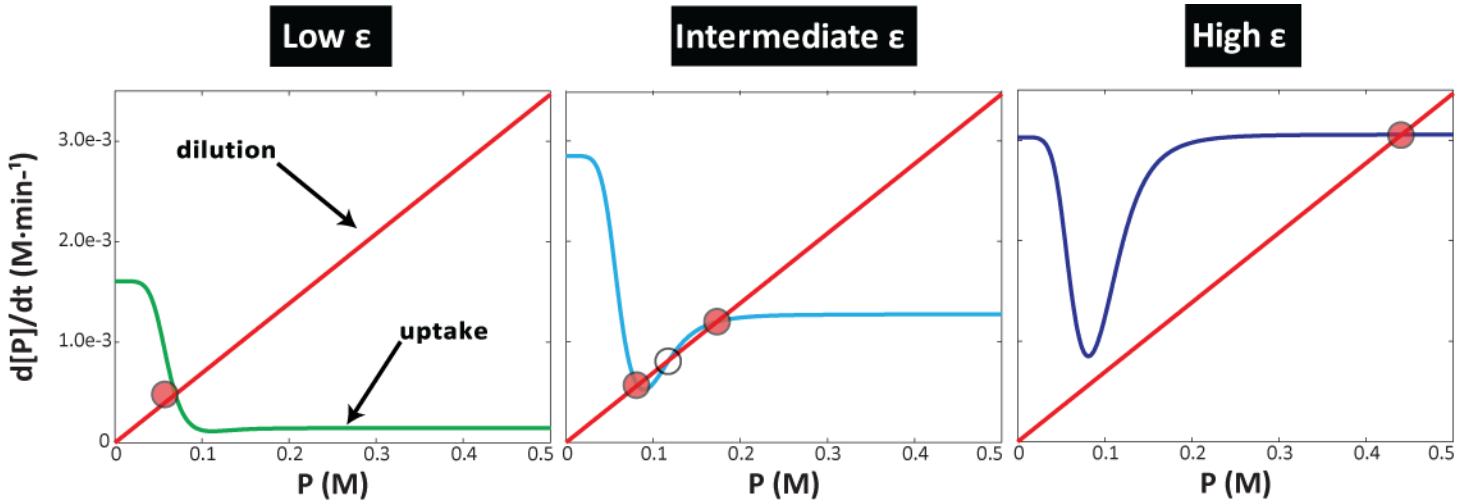

Figure 3.1: ***Figure 3.1: Vector Field Map for the PHO signaling model.***

Calculation of fixed point stabilities. A full understanding of the steady state behavior of the system requires the determination of the stability of each fixed point. The stability of any given fixed point can be determined from the eigenvalues of the Jacobian of the system. For the PHO model, the Jacobian is:

$$J_F = \begin{pmatrix} \frac{\partial \dot{H}}{\partial H} & \frac{\partial \dot{H}}{\partial L} & \frac{\partial \dot{H}}{\partial P} \\ \frac{\partial \dot{L}}{\partial H} & \frac{\partial \dot{L}}{\partial L} & \frac{\partial \dot{L}}{\partial P} \\ \frac{\partial \dot{P}}{\partial H} & \frac{\partial \dot{P}}{\partial L} & \frac{\partial \dot{P}}{\partial P} \end{pmatrix} = \begin{pmatrix} -g & 0 & \frac{\beta_L \left(\frac{T_L}{P}\right)^{n_L} n_L}{\left(\left(\frac{T_L}{P}\right)^{n_L}+1\right)^2 P} \\ 0 & -g & \frac{\beta_H \left(\frac{P}{T_H}\right)^{n_H} n_H}{\left(\left(\frac{P}{T_H}\right)^{n_H}+1\right)^2 P} \\ \frac{\varepsilon V_L}{\varepsilon + k_L} & \frac{\varepsilon V_H}{\varepsilon + k_H} & -g \end{pmatrix} \quad (3.5)$$

Numerical determination of the eigenvalues of the Jacobian at specific internal and external phosphate values showed that in low or high phosphate, the single fixed point is stable. At 150 μM external phosphate, of the three fixed points, two are stable (red circles) and one is unstable (unfilled circle) that defines a phase transition. At internal phosphate levels above this point the system will move towards the higher stable steady state and at internal phosphate conditions below this point the system will move towards the lower steady state.

Table 3- 1: Parameters and variables used in the phosphate signaling model.

Parameters	Value/Units	Notes/References
β_L	6.9 x 10^{-3} min^{-1}	*
β_H	6.9 x 10^{-3} min^{-1}	*
γ	6.9 x 10^{-3} min^{-1}	†
T_L	0.11 M	‡
T_H	0.06 M	‡
n_L	6	‡
n_H	6	‡
V_L	3.82 x 10^{-3} M•min^{-1}	(Wykoff and O'Shea, 2001)
V_H	3.06 x 10^{-3} M•min^{-1}	(Wykoff and O'Shea, 2001)
k_L	2.5 x 10^{-4} M	(Wykoff and O'Shea, 2001)
k_H	9 x 10^{-6} M	(Wykoff and O'Shea, 2001)
System Control Variable (time independent)		
ε	M	Fixed at t = 0
System Variables (time-dependent)		
L	Fraction Max	§
H	Fraction Max	§
P	M	**

* Calculated to give maximal measured uptake rates at maximum transporter concentration.

† Based on 100 minute doubling time, i.e. ln(2)/doubling time.

‡ Fit values.

§ Fraction of maximum concentration, i.e. high Pi for L and no Pi for H (see methods).

** Modeled steady-state values.

One-Dimensional Bifurcation analysis. In reality, what we are interested in understanding is the relationship between external phosphate (E) and the state of the PHO pathway. The internal phosphate concentration, concentration of high affinity transporters, and concentration of low affinity transporters are all linked to one another. Therefore, by solving for the steady state concentration of any one of these time dependent species, we can solve for the other two. Although no analytical solution exists for equation 3.4, it is possible to numerically calculate the value of P as a function of E. Additionally, we can calculate both H and L at these P values using equations 3.1 and 3.2.

I have solved for the steady state internal phosphate, Pho84 and low affinity transporter concentrations as functions of external phosphate. I used a set of parameters combining both experimentally measured parameters, and for unknown parameters, values that were fit to the observed behavior of the PHO pathway (Table 3.1). As can be seen in Figure 3.2, there is a range of external phosphate concentrations for which three steady states exist for Pho84, low affinity transporters and the internal phosphate concentration (yellow area). These correspond to the two stable and one unstable steady state indicated in Figure 3.1 and determined using equation 3.5.

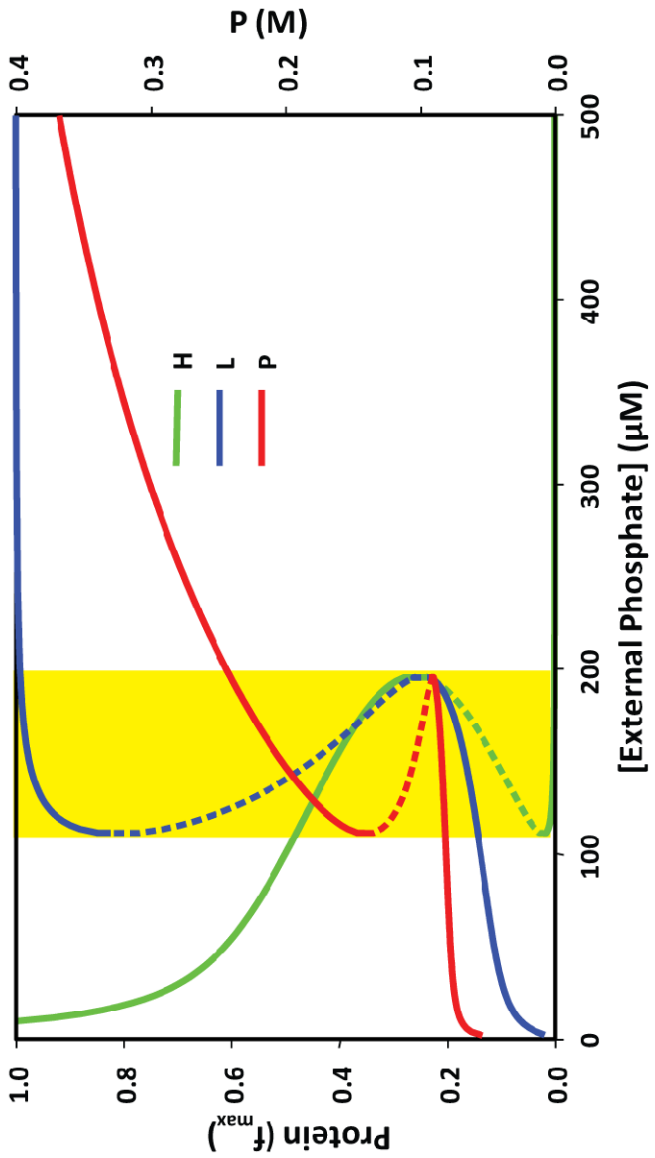

Figure 3.2: Bifurcation Analysis of the PHO Signaling model.

The mathematical model described suggests that the positive feedback in the PHO pathway due to the down-regulation of low affinity transporters can lead to a bistable system. Additionally, the model provides a framework for understanding the pathway and makes specific predictions about requirements for bistability as well as the behavior of the system when perturbed.

Figure Legends

Figure 3.1: Vector Field Map for the PHO signaling model. The rate of change of internal phosphate ($^{dP}/_{dt}$) is plotted versus the internal phosphate concentration at three different external phosphate concentrations (1μM, 150μM and 1mM). The dilution components of $^{dP}/_{dt}$ (equation (3.4)) is indicated in red. The uptake components of $^{dP}/_{dt}$ are indicated in green, cyan and blue for low, intermediate and high external phosphate respectively. Parameter values from Table 3.1 were used for plotting.

Figure 3.2: Bifurcation Analysis of the PHO Signaling model. Bistability in the PHO pathway depends on the concentration of external phosphate. Steady state amounts of the three time-dependent species are plotted as a function of external phosphate. The fraction of maximum levels of high and low affinity transporters (H and L) are plotted on the left y-axis with green and blue curves respectively. The concentration of internal phosphate is plotted on the right y-axis in red. As external phosphate ranges from zero to 500μM, the system enters a region of bistability defined by two saddle node bifurcations (highlighted in yellow). For external phosphate values within the bistable region, there are three fixed points, two of which are stable

(solid lines) and one of which is unstable (dashed lines).

Chapter IV: Model Predictions

Introduction

One of the benefits of having a mathematical model of a complex system is that it helps to understand complex behaviors that may not be initially intuitive. For example, by fitting model parameters, the model may point out specific features of a system that are required to obtain specific behaviors. Additionally, the model may help to make predictions about the behavior of a system when the system is perturbed in some way. If these perturbed conditions were not included in the original model, they lend support to veracity of the model. Finally, the model may help to explain the source of previously observed system behaviors.

Results

Analysis of positive feedback mutant. One suggestion of the model is that bistability depends on positive feedback due to low affinity transport inhibition. By setting the value of T_L in the model to zero, I was able to simulate the deletion of *SPL2*. Figure 4.1 shows the steady-state concentration of Pho84 as a function of external phosphate with the value of T_L set to zero. As can be seen, the model now predicts that *PHO84* expression is no longer either bistable or ultra-sensitive. To test this, I deleted *SPL2* in reporter strain EY2415 and analyzed steady state *PHO84* expression as a function of phosphate concentration by flow cytometry in this strain (EY2416). As predicted, the Pho84 response is no longer bimodal or hysteretic (Figure 4.2) (Wykoff et al., 2007).

The PHO pathway is bistable. Although the experiments discussed in chapter two showed that *PHO84* expression is bistable, they did not address the PHO pathway as a whole. It is possible that *PHO84* is expressed in a bistable manner even though the full PHO pathway is not. The model predicts that both internal phosphate and Spl2 levels should also be bistable over the same range of [external phosphate] as Pho84 (see Figure 3.2). Additionally, for any given cell, the levels of Pho84 and Spl2 should always be the same, i.e. cells that express Pho84 should express Spl2 and vice versa.

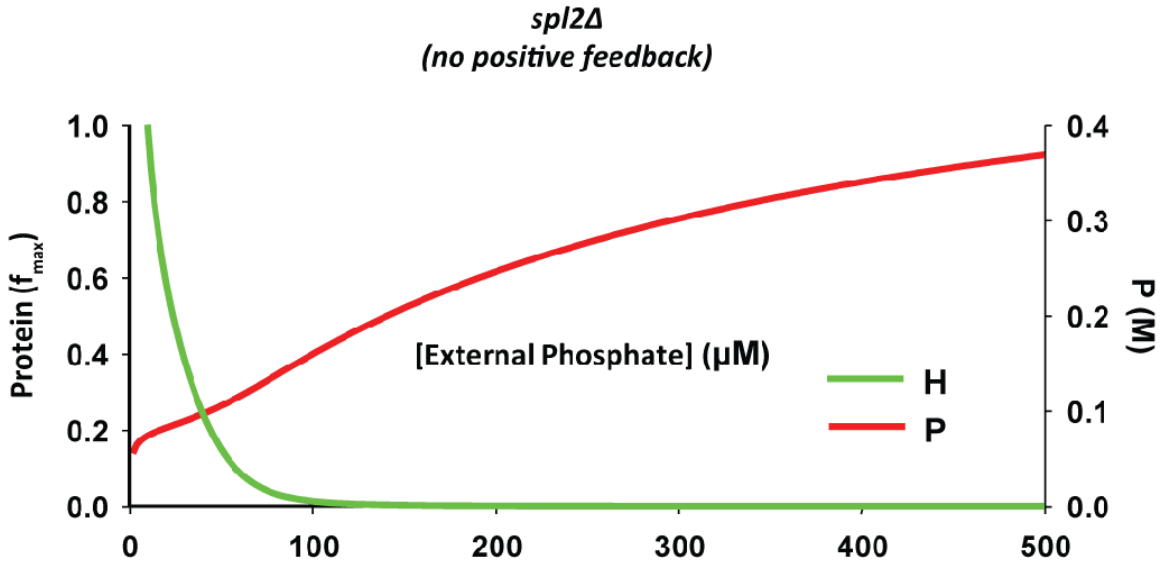

Figure 4.1: Bifurcation Analysis of PHO Signaling Model in the Absence of Positive Feedback Shows Loss of Bistability.

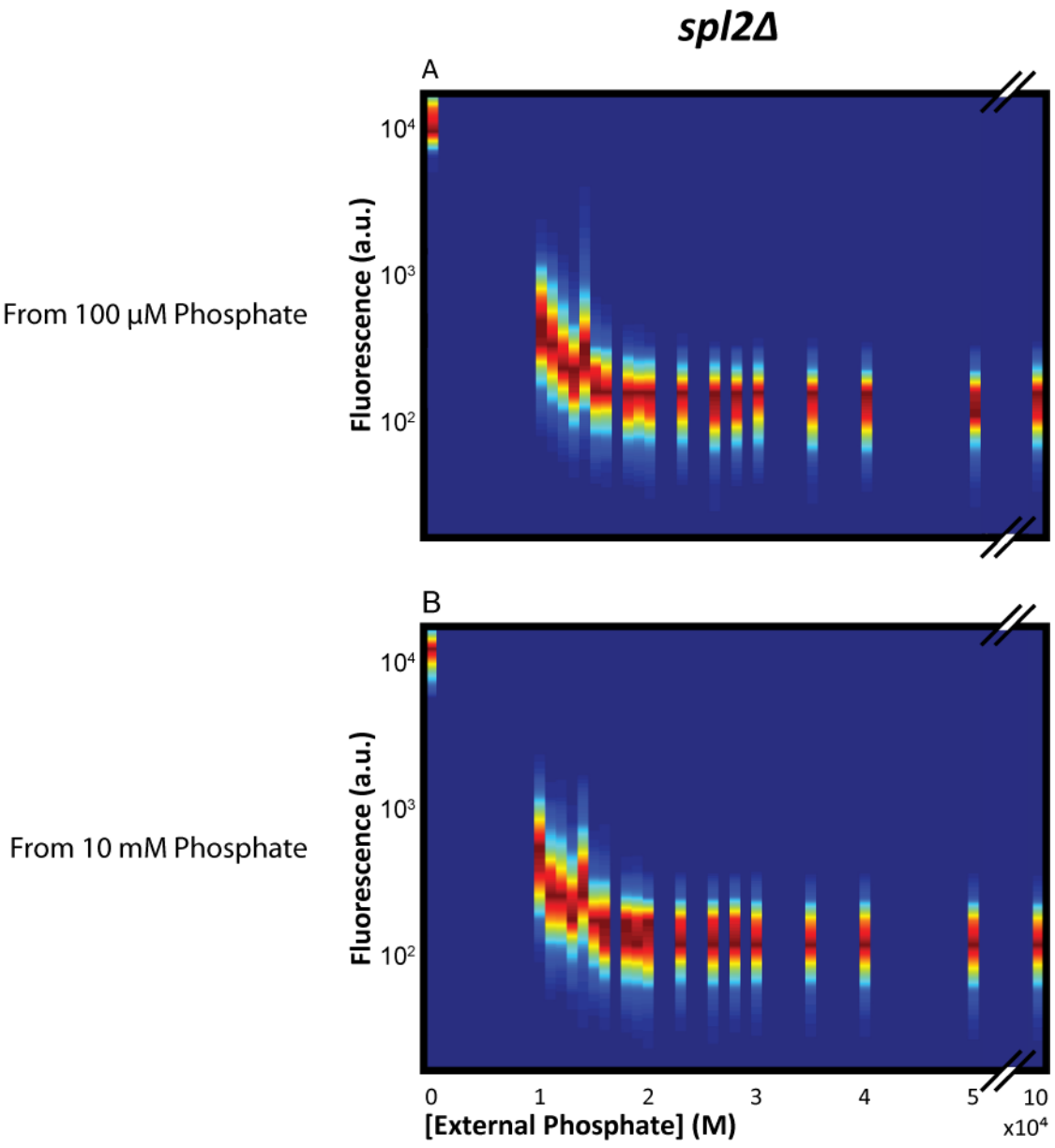

Figure 4.2: Loss of Positive Feedback abolishes bistability.

Using a reporter strain (EY2416) with *PHO84* and *SPL2* transcriptional reporters (CFP and YFP respectively) in the presence of functional copies of both genes, I have measured the levels of *PHO84* and *SPL2* expression in single cells through a range of external phosphate conditions. At all phosphate concentrations tested, *PHO84* and *SPL2* expression were exactly in sync with one another (Figure 4.3).

PHO states are heritable. The model predicts that internal phosphate levels should inversely correlate with *PHO84* and *SPL2* expression, i.e. cells that express both Pho84 and Spl2 should have lower internal phosphate levels. Unfortunately, it is not technically possible to measure internal phosphate levels in single cells. It is possible to, at least qualitatively, gain information on the internal phosphate level of cells by determining the activity of the transcription factor, Pho4. Because Pho4 is regulated primarily at the level of localization, its activity level can be determined by assaying its localization. When the PHO pathway is active, Pho4 is localized to the nucleus and when it is inactive it is localized to the cytoplasm (O'Neill et al., 1996). As a means to correlate activity of the PHO pathway with the expression level of *PHO84*, I engineered a strain bearing three different fluorescent reporters (EY2417). Pho4 was fused to citrine-YFP, to determine its localization. To measure *PHO84* expression, a *PHO84* promoted cerulean CFP construct was targeted to the *HIS3* locus. Finally, to accurately determine the location of the nucleus, the nuclear

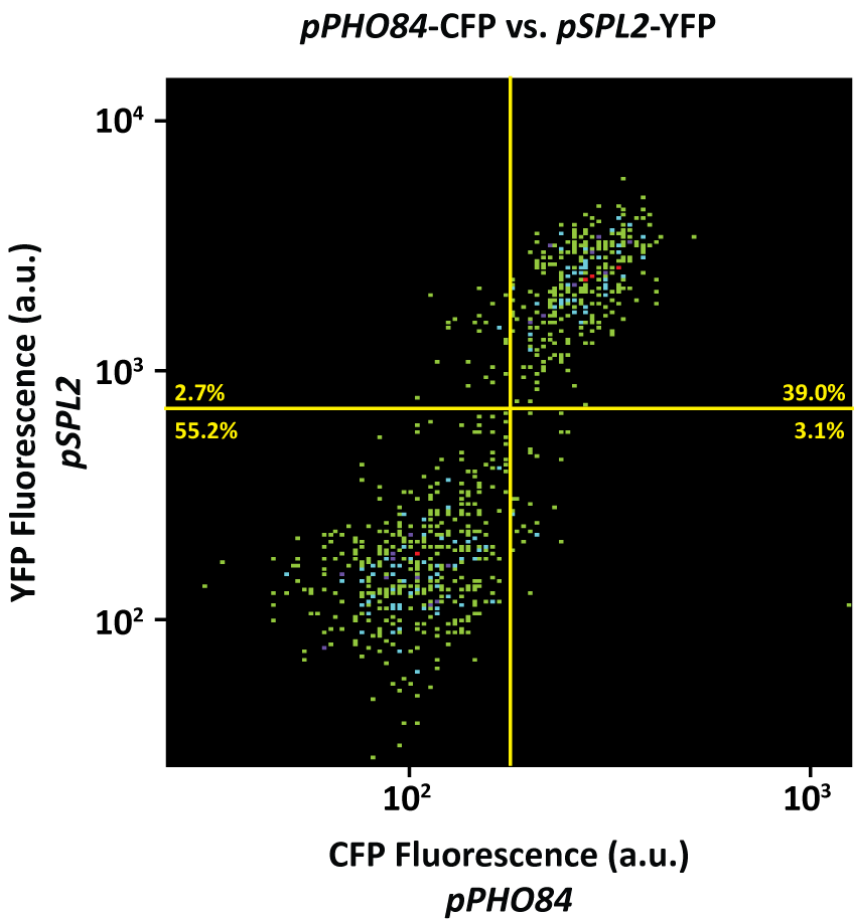

Figure 4.3: Expression of PHO84 and SPL2 is correlated.

localized protein, Nhp6a was fused to a yeast codon optimized variant of the red fluorescent protein, mCherry (Campbell et al., 2002).

This strain was then grown in a microfluidic device while intermediate phosphate media was flowed over the cells. The device maintains all cells in a single focal plane for easier analysis. The cells were then imaged for all 3 fluorescent proteins at 15 minute intervals for 18 hours. As predicted, there was a perfect correlation between *PHO84* expression and Pho4 localization. By monitoring *PHO84* expression and Pho4 localization over time, an additional surprising feature of the PHO pathway was uncovered. Cells in a microfluidic device were switched from high phosphate media to a concentration of phosphate where the PHO pathway was activated in approximately 50% of the cells. Within about 10 minutes of the phosphate switch, Pho4 relocalized to the nucleus in about 50% of the cells. Consequently, approximately two hours later, CFP fluorescence could be detected in each cell for which Pho4 had relocalized to the nucleus. By continuing to monitor the cells over time, it became clear that once the initial PHO switch had been set, the state of the PHO pathway was heritable. That is, cells in which the PHO pathway had been activated gave rise to cells in which the pathway was on and cells in which the PHO pathway had not been activated gave rise to cells in which the PHO pathway was not activated (Figure 4.4).

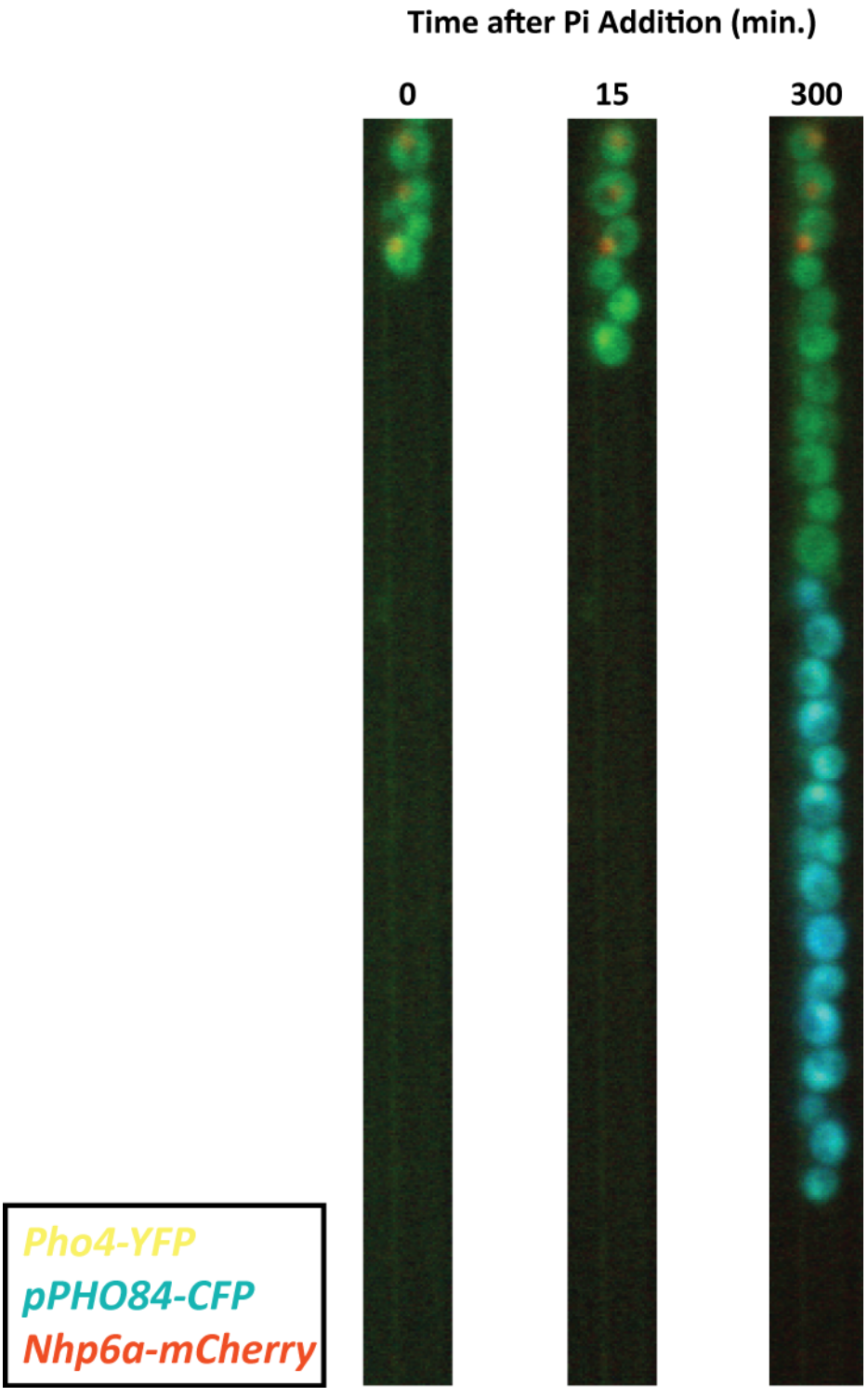

Figure 4.4: Microscopic Analysis Shows Heritability of the State of the PHO Pathway.

Bistability depends on specific T_L:T_H ratios. Observations of vector field plots (such as in Figure 3.1-B) show that bistability depends upon a "dip" in the phosphate uptake rate at intermediate internal phosphate levels. This dip is due to a decrease in the level of net phosphate uptake due to down-regulation of low affinity transporters. Nevertheless, down-regulation of low affinity transport, *per se*, does not lead to a dip in the phosphate uptake rate. In fact, increases in the level of high affinity transport can easily compensate for a decrease in low affinity transport, yielding no net change in the total phosphate uptake rate (see Figure 4.5-A). Only when the inhibition of low affinity transport occurs at an internal phosphate concentration above that at which Pho84 is induced, do we see a dip in net phosphate uptake. Therefore, the PHO signaling model predicts a specific difference in the values of T_H and T_L. Specifically, the model requires that for the existence of bistability in the pathway, the value of T_H must be below that of T_L (see Figure 4.5).

Bifurcation analysis of induction thresholds. Although we can see qualitatively that there is a requirement for a difference in the values of T_H and T_L, full understanding of the model and its predictions requires a more quantitative assessment of the effects that T_H and T_L can have on the behavior of the system. Therefore, I analyzed the system for a range of T_L:T_H ratios. To make the analysis both computationally

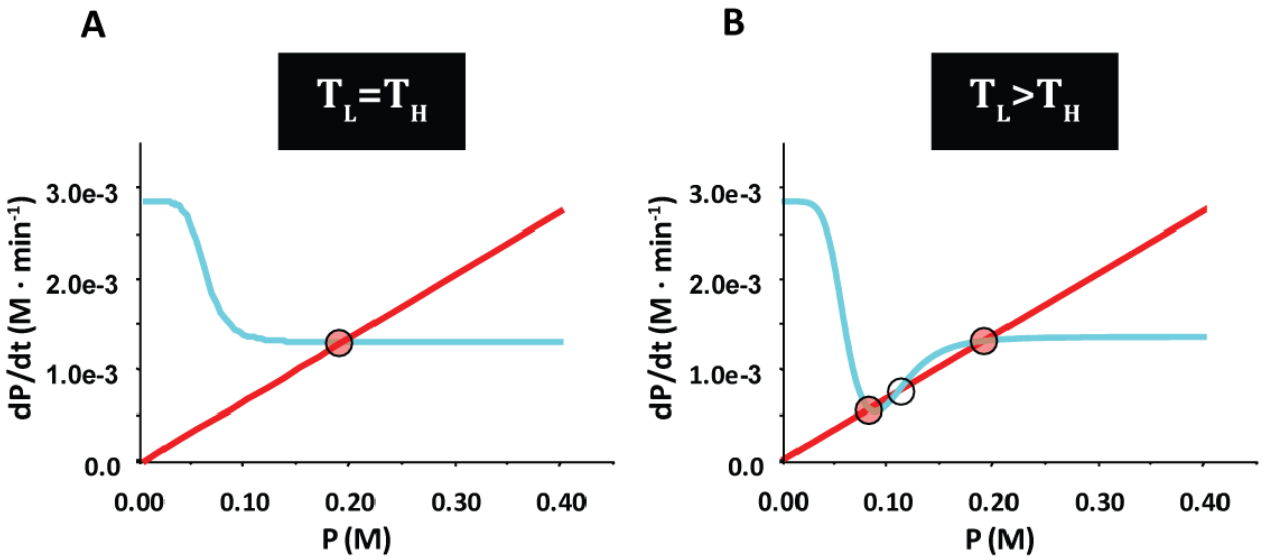

$$\frac{\partial H}{\partial t} = \frac{\beta_H}{\left(\frac{P}{T_H}\right)^{n_h} + 1} - H\gamma$$

$$\frac{\partial L}{\partial t} = \frac{\beta_L}{\left(\frac{T_L}{P}\right)^{nl} + 1} - L\gamma$$

$$\frac{\partial P}{\partial t} = \frac{H\varepsilon V_H}{\varepsilon + k_H} + \frac{L\varepsilon V_L}{\varepsilon + k_l} - P\gamma$$

Figure 4.5: Figure 4.5: Vector Field Maps at Different TH:TL Ratios.

less intensive as well as to make the results easier to interpret, I changed the T_L:T_H ratio by varying the value of T_L while maintaining T_H at a constant value*. As discussed in chapter three, equation (3.4) equals 0 at steady state. As can be seen in Figure 3.1, only for certain values of external phosphate do three fixed points exist. If we imagine varying values for external phosphate, we can see that at the point the system converts from one to three fixed points, the uptake curve is tangent to the dilution curve, i.e. the derivatives of the uptake and dilution curves are equal:

$$\frac{\varepsilon\left(-\frac{\beta_H n_H \left(\frac{P}{T_H}\right)^{-1+n_H} V_H}{(\varepsilon+k_H)\left(1+\left(\frac{P}{T_H}\right)^{n_H}\right)^2 T_H}+\frac{\beta_L n_L T_L \left(\frac{T_L}{P}\right)^{-1+n_L} V_L}{(\varepsilon+k_L)P^2\left(1+\left(\frac{T_L}{P}\right)^{nl}\right)^2}\right)}{\gamma}=\gamma \qquad (4.1)$$

To visualize the system, I solved the system of equations comprising equations (3.4) and (4.1) over a range of P values and parametrically plotted the results, i.e. plotted the points (E (P), T_L (P)) over the (E,T_L) plane (Figure 4.6)†.

* See Matlab code in the appendix for details.

† For reasons of computational simplicity, I actually solved for P and E over a range of T_L values. See Matlab code in appendix for details.

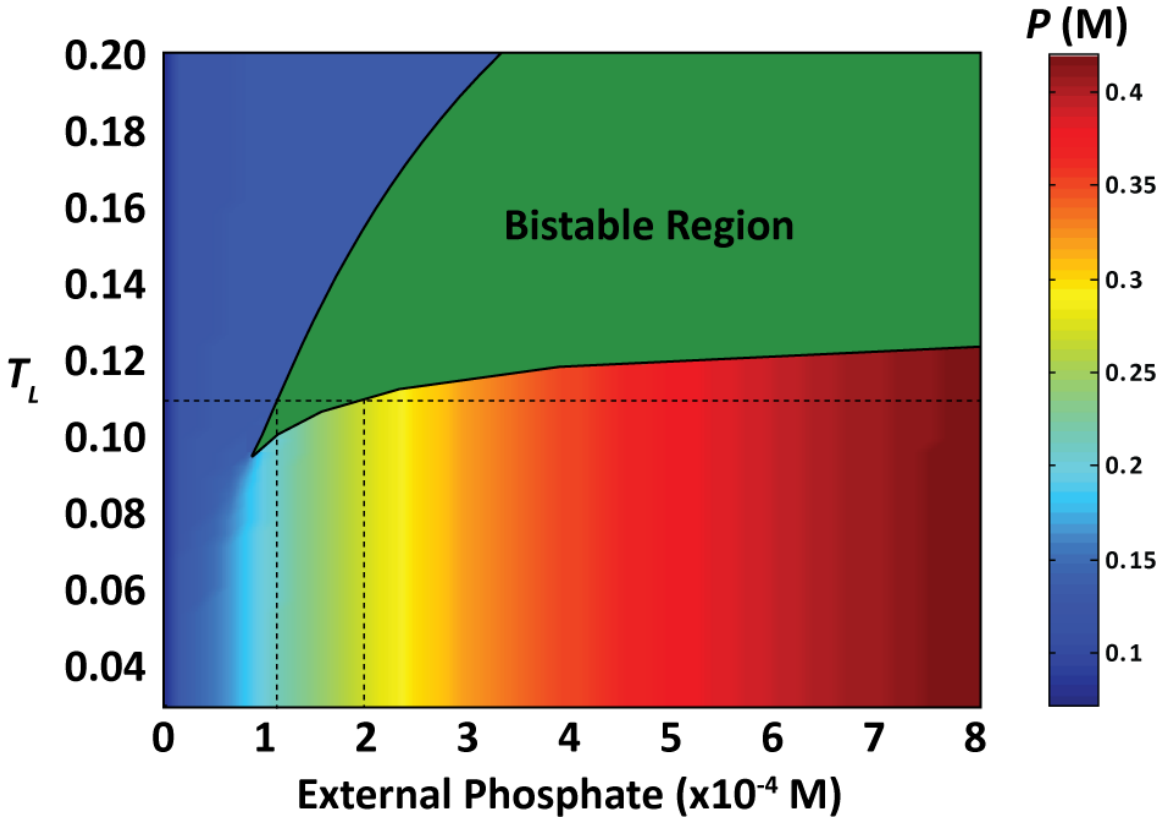

Figure 4.6: Parametric Plot of PHO Model.

As can be seen in Figure 4.6, at T_L values below approximately 0.09 (equivalent to a T_L:T_H ratio of 1.5), no bistable region exists. At T_L values above approximately 0.13, an upper bound for the region of bistability ceases to exist thereby rendering the system monostable (with an active PHO pathway). This outcome can alternatively be reached by lowering the value T_H, which is analogous to deleting *PHO84*.

Measurement of induction kinetic parameters. Measurement of the kinetic parameters relating expression of the transporters to [internal phosphate] is not possible in the context of the full PHO pathway. In the PHO pathway, at least three time-sensitive species (L, H, and P) are varying at the same time. Furthermore the production rates of these species depend on one another (see equations 3.1, 3.2 and 3.3). Therefore, it is not possible to measure directly the dependency of one of the species on another. One way to get around this problem is to physically separate the processes such that the production rates of each of the species does not depend on the levels of any of the other varying species. A parameter, such as [external phosphate], can then be varied while the steady state level of any of the three species is measured. For example, by deleting *PHO84* and *SPL2*, the three rate equations become:

$$H = 0; \quad \text{Constant \&=0} \tag{4.2}$$

$$\frac{\partial L}{\partial t} = \beta L - L\gamma = 0 \therefore L = \frac{\beta_L}{\gamma}; \quad \text{Constant} \tag{4.3}$$

$$\frac{\partial P}{\partial t} = \frac{\varepsilon V_L}{\varepsilon + k_L} - P\gamma = 0 \therefore P = \frac{\varepsilon V_L}{\gamma\left(\varepsilon + k_L\right)} \tag{4.4}$$

To measure the kinetic parameters relating expression of the transporters to [internal phosphate] I replaced the *PHO84* and *SPL2* ORFs with CFP and YFP respectively (EY2418). I predicted that this strain would no longer exhibit any feedback in the PHO pathway as there will be no functional copies of either *PHO84* or *SPL2* and therefore, presumably, no feedback.

Surprisingly, when I measured the system response in this double deletion strain (Figure 4.7), I found that the pathway responded in a bistable fashion. This was particularly surprising given that deletion of the *SPL2* completely abolished bistability (Figure 4.2).

This result likely indicates that there are, in fact, multiple feedback loops present in the PHO pathway that were not apparent in the presence of the two main loops.

Understanding noise effects in the PHO Pathway. One feature of a bistable system is that for any given input trajectory, there should only be a single output. Nevertheless, biological systems are far from "perfect"; noise can introduce cell to

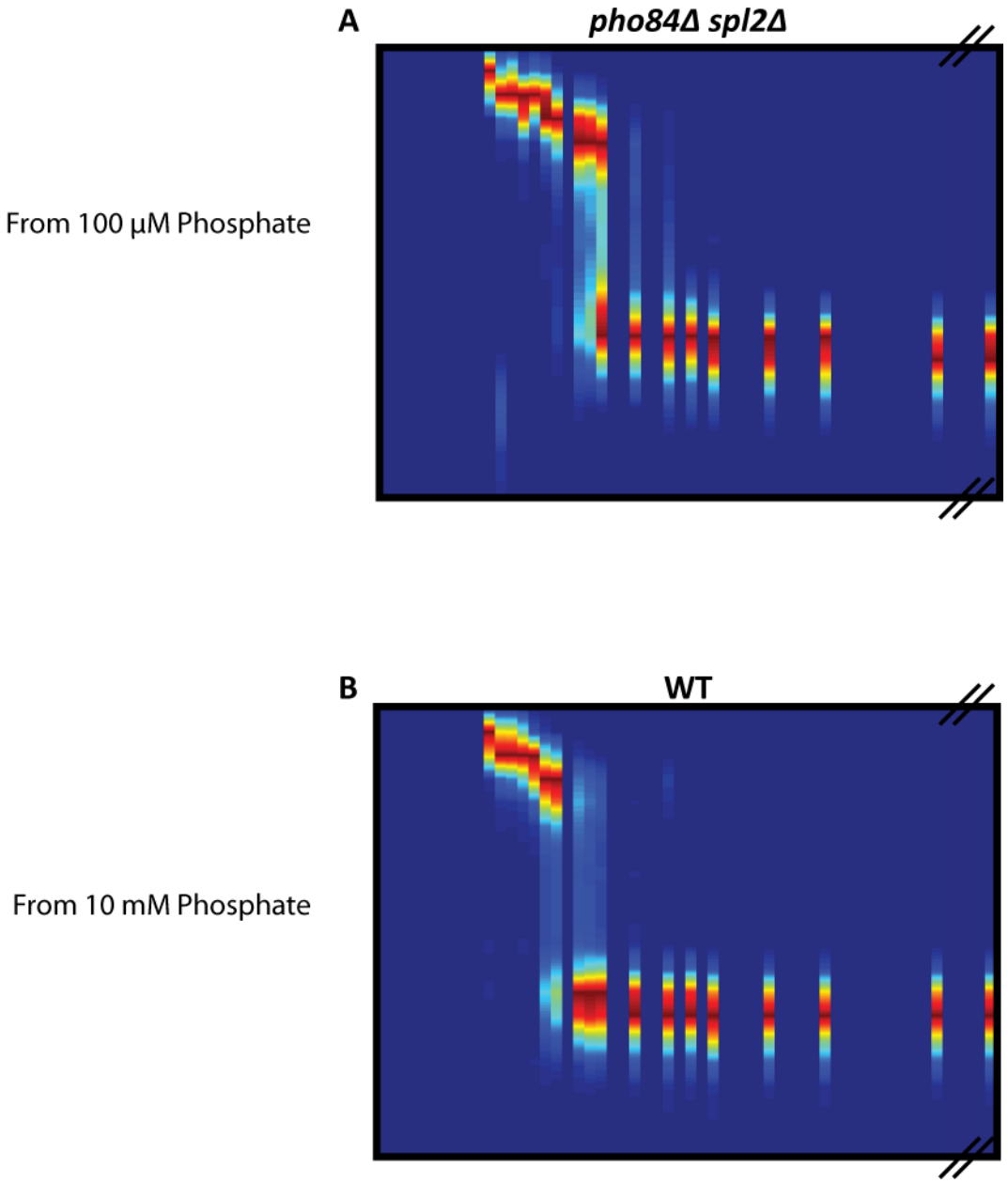

Figure 4.7: Bistability in a pho84Δ spl2Δ Strain.

cell differences at a given input trajectory that would not be seen for a noiseless system. For example, although the PHO pathway model predicts that for any given external phosphate concentration, all cells in a culture would be either ON or OFF for *PHO84* expression, this is clearly not the case; some cells are ON while others are OFF at certain external phosphate concentrations. The reason for this is likely stochastic fluctuations in various system components. If we consider two cells with slightly different parameters, we see that they respond to slightly different [external phosphate]. At high or low phosphate, both cells are OFF for *PHO84* expression and at low phosphate, both are ON. On the other hand, at the intermediate phosphate concentration chosen, only cell 1 is ON. Consequently, measured hysteresis appears lower than it actual is because at any given phosphate concentration, only some of the cells in the population are within their bistable range.

Whatever cell to cell variability in the PHO pathway that exists seems to take a long time to become established. As mentioned above, when single cells are followed through time in intermediate phosphate by either microscopy or cell sorting experiments, the rate of switching between the ON and OFF populations is very slow. This suggests that cells tend to inherit the stochastic state of their parents. When analyzed at the single cell level, though, the Pho system should show increased measured hysteresis.

Figure Legends

Figure 4.1: Bifurcation Analysis of PHO Signaling Model in the Absence of Positive Feedback Shows Loss of Bistability. Steady state amounts of the two time-dependent species are plotted as a function of external phosphate for an *spl2Δ* strain. The fraction of maximum levels of high affinity transporters (H) is plotted on the left y-axis with green curves. The concentration of internal phosphate is plotted on the right y-axis in red. At all external phosphate concentrations between zero and 500 μM K_2HPO_4 only a single (stable) fixed point exists.

Figure 4.2: Loss of Positive Feedback abolishes bistability. *spl2Δ* strain EY2416, bearing *PHO84*-promoted Cerulean CFP at the *URA3* locus and *SPL2*-promoted Citrine YFP at the *HIS3* locus, was grown overnight to mid-log phase (OD600 = 0.2) in synthetic media supplemented with 10 mM K_2HPO_4. Cultures were then washed and resuspended in fresh media containing either 100 μM or 10mM K_2HPO_4, grown for 4 hours and then diluted into fresh synthetic media supplemented with K_2HPO_4 at concentrations ranging from zero to 1 mM. To prevent phosphate depletion, cells were inoculated at densities so that after 18 hours of growth there were approximately 5 x 10^4 cells/ml. For each culture, density maps display the fraction

of cells showing the indicated median YFP fluorescence value for all phosphate concentrations tested.

Figure 4.3: Expression of PHO84 and SPL2 is correlated. Strain EY2415, bearing *PHO84*-promoted Cerulean CFP at the *URA3* locus and *SPL2*-promoted Citrine YFP at the *HIS3* locus, was grown overnight to mid-log phase (OD600 = 0.2) in synthetic media supplemented with 10 mM K_2HPO_4. Cultures were then diluted into fresh synthetic media supplemented with 150 μM K_2HPO_4. To prevent phosphate depletion, cells were inoculated at densities so that after 18 hours of growth there were approximately 5 x 10^4 cells/ml. Cells were then analyzed on a Becton-Dickinson LSR2 flow cytometer for both CFP and YFP fluorescence. Each dot on the plot shows the fluorescence data of a single cell. Dots are color-coded based on the density of cells in a given region. The plot is divided into quadrants based on levels of CFP and YFP fluorescence. Starting from the top left quadrant and moving clockwise, the quadrants represent low CFP-high YFP; high CFP-high YFP; high CFP-low YFP and low CFP-low YFP fluorescence. Percent of total number of cells residing in each quadrant is indicated.

Figure 4.4: Microscopic Analysis Shows Heritability of the State of the PHO Pathway. EY2417 was grown overnight in synthetic media supplemented with 10mM K_2HPO_4

to mid-log phase and then loaded into a microfluidic device that mechanically forces cells to grow in a line. This way, cell lineages can easily be determined. The device was mounted on a Zeiss Axiovert 200M microscope. Cells were initially grown for two hours in the microfluidic device while high phosphate media was perfused over them. After two hours, the perfusion media was switched to synthetic media supplemented with 150 μM K_2HPO_4. At 15 minute intervals, cells were imaged with a Zeiss 63x objective at CFP, YFP and RFP wavelengths. The three images were false colored and overlaid. Images from zero, 15 and 300 minutes following the switch to 150 μM perfusion media are shown.

Figure 4.5: Vector Field Maps at Different T_H:T_L Ratios: The rate of change of internal phosphate ($^{dP}/_{dt}$) is plotted versus the internal phosphate concentration at in intermediate phosphate (ε = 150μM). The dilution components of $^{dP}/_{dt}$ (equation (3.4)) is indicated in red. The uptake component of $^{dP}/_{dt}$ is indicated in blue. Values for T_L are 0.16 (panel A) and 0.11 (Panel B). All other parameter values are from Table 3.1.

Figure 4.6: Parametric Plot of PHO Model. Points [E(P), T_L(P)] in the (E, TL) plane that define saddle node bifurcations are plotted over values of P. These points

define a boundary of bistability. Within the curves defined by these points lies a region of bistability (indicated in green). Outside of this region, the system is monostable and no saddle node bifurcations exist. In the monostable region, the value of P is indicated with color. The value of T_L (0.11) that was fit to data is indicated by a horizontal dashed line. The range of bistability at this value of T_L is indicated by dashed vertical lines dropping from the horizontal line.

Figure 4.7: Bistability in a pho84Δ spl2Δ Strain. *pho84Δ spl2Δ* strain EY2418, was grown overnight to mid-log phase (OD_{600} = 0.2) in synthetic media supplemented with 10 mM K_2HPO_4. Cultures were then washed and resuspended in fresh media containing either 100 μM or 10mM K_2HPO_4, grown for 4 hours and then diluted into fresh synthetic media supplemented with K_2HPO_4 at concentrations ranging from zero to 1 mM. To prevent phosphate depletion, cells were inoculated at densities so that after 18 hours of growth there were approximately 5 x 10^4 cells/ml. For each culture, density maps display the fraction of cells showing the indicated median YFP fluorescence value for all phosphate concentrations tested.

Chapter V: Discussion

Function of bistability in the Pho pathway.

Although the presence of a bistable response to changing phosphate conditions is apparent, the function is not at all clear. Presumably, there are emergent properties of this bistable system that confer a selective advantage to cells. Alternatively, bistability may occur as a necessary "side effect" of another selected feature of the pathway.

Environmental phosphate. *Saccharomyces* is adept at living in widely varying environments. Although *Saccharomyces* can utilize a wide range of molecules to provide its energy and nutritional requirements, it can survive, when necessary, on a remarkably small number of nutrients. In addition to an energy source (such as glucose), Saccharomyces also requires only the following small number of additional nutrients (Table 5.1).

Table 5.1: Nutritional requirements of yeast

Carbon source	Chloride	Magnesium
Potassium	Phosphate	Sulfate
Sodium	Nitrogen source	Trace minerals

Of these, phosphate stands out as being required in large amounts, yet with limited availability. Even when phosphate ions are plentiful in the environment, they are

rapidly rendered insoluble and therefore unavailable for use by the organism (Deacon, 2006).

It seems likely that the combination of large usage requirements (which may lead to rapid environmental depletion) combined with environmental scarcity would lead to a situation where cells need to respond rapidly to changes in environmental phosphate availability. For example, upon depletion of phosphate from growth media, yeast cells quickly begin to utilize their internal phosphate stores, which are capable of maintaining growth until the stores are depleted in approximately 30 minutes (Thomas and O'Shea, 2005). Nevertheless, this is likely not enough time for the cell to reposition itself for growth in a low phosphate environment, i.e. to build up maximal levels of Pho84 and other enzymes necessary for phosphate scavenging.

One way to mitigate a requirement for a rapid cellular response upon environmental phosphate depletion would be to anticipate and prepare for environmental changes. Then, rather than needing to respond rapidly to environmental changes, a cell would already be primed for the new condition.

This, in fact, could be a function of bistability in the PHO pathway. A decrease in environmental phosphate from high to intermediate levels may be an indication that environmental phosphate levels may soon drop to even lower levels. The switch-

like behavior provided by a bistable pathway would allow the pathway to "trip," leading to full pathway activation. That way, when environmental phosphate levels reach a critical level, cells would already be "primed" for life in this new phosphate limited environment.

Multiple Feedback Loops

Surprisingly, when both the negative and positive feedback loops of the PHO pathway were deleted, we found that the response to phosphate starvation was still bistable. Although we do not know the actual source of bistability in the absence of the feedback loops, it seems likely that additional feedback loops are operating. Upon deletion of the main negative feedback loop, i.e. the *PHO84*-dependent loop, the PHO pathway is monostable and active. Upon deletion of the main positive feedback loop, i.e. the *SPL2*-dependent loop, the PHO pathway responds to phosphate depletion in a graded manner. Both of these responses were predicted by the PHO model. Nevertheless, the pathway returned to a bistable state when both feedback loops were deleted.

This points out an important feature of feedback systems. Feedback loops can have strong effects on the outcome of a signaling system, as evidenced by the results of deleting either *PHO84* or *SPL2*, and therefore need to be carefully balanced. This is also evidenced by the results of the two-dimensional bifurcation analysis shown in Figure 4.6. We can think of changes in the T_L:T_H ratio as changes in the positive:negative feedback ratio. Very small shifts in the value of T_L have significant effects on pathway behavior. If the value of T_L is raised slightly, the system is moved

into a region of effective monostability. On the other hand, if the value of T_L is lowered slightly, the system is moved into a region of graded responses.

On the other hand, changes to the values of TL and TH that do not change their ratio, have much more suttle effects on the response of the pathway; primarily shifting the range of the bistable region, while maintaining its width. Therefore, deletion of either *PHO84* or *SPL2* have such drastic effects on the behavior of the PHO pathway, not because the feedback loops are themselves essential, but rather because the balance of positive and negative feedback is shifted. The additional putative feedback loops are presumably still present and functional in single knockout strains, they just can't compensate for the feedback imbalance.

Unfortunately, the lack of knowledge about the nature of the additional putative feedback loops makes it difficult to test ideas about feedback balancing. Nor is it possible to address questions about possible properties provided to the system due to the presence of multiple layers of feedback (vs. just one positive and one negative feedback loop). Therefore, a prime future direction should be to identify the source, mechanism and function of these additional feedback loops.

Appendix

Yeast strains

To integrate the $_{P}$*PHO84* reporter at the yeast *URA3* locus in strain EY1995, plasmid EB1632 (pFA6ayEGFP-KANMX6) was used as a template to precisely replace the open reading frame (ORF) of *PHO84* using a PCR-based inactivation protocol (Kitada et al., 1995; Longtine et al., 1998). Genomic DNA from this strain was isolated and oligonucleotides cg**ggatcc**ccacattgaacttttcacttcg and cc**gcggccgc**ttatttgtacaattcatccatacc were utilized to amplify this genomic region and clone it into pRS306 (Sikorski and Hieter, 1989). This plasmid (EB1656) was then linearized with *Stu*I, transformed into yeast strains that had a wild-type *PHO84* locus, and selected for by uracil prototrophy (Wykoff et al., 2007).

To generate multi-reporter strains, fusion PCR (Amberg et al., 1995) was used to generate $_{P}$*PHO84* and $_{P}$*SPL2* fluorescent protein fusions. The *PHO84* and *SPL2* promoters were amplified from EY690 (W303) genomic DNA using fusion primers 1 and 2 or 3 and 4 (Table A.1) respectively. Fluorescent protein ORFs citrine-YFP and cerulean-CFP were amplified by PCR using oligonucleotides 5 and 6 or 7 and 6 (Table A.1) from plasmids pKT211 and pKT270 respectively (Sheff and Thorn, 2004). These four PCR products were gel isolated, combined in all possible promoter/reporter combinations and reamplified with oligonucleotides 1 and 6 (for *PHO84*) or oligonucleotides 3 and 7 (for *SPL2*). Following secondary PCR reactions

the products were digested with *AscI* and *SalI* and cloned into plasmid pKT211 that had been linearized with *AscI* and *SalI*. PCR products were generated using primers 8 – 13. Integration of the reporters at the *HIS3* and *URA3* loci was performed by transformation of EY690 with these PCR products followed by selection for histidine prototrophy. Strain EY2415 bearing both $_P$*PHO84*-cerulean and $_P$*SPL2*-citrine reporters was generated by mating strains EY2407 and EY2414. *Spl2Δ* reporter strain EY2416 was generated by mating of EY2415 to the *spl2Δ* strain EY1872 (Wykoff et al., 2007).

Three-color strain EY2417 was generated by mating of EY2414 to EY2150 (Harold Kim, Unpublished) followed by successive selection and screening for the correct genotype.

To replace the *pho84* ORF with cerulean-CFP, the cerulean-CFP ORF (with yeast G418 resistance marker) was amplified from plasmid pKT308. To replace the *spl2* ORF with citrine-YFP, the citrine-YFP ORF (with yeast HIS3 marker) was amplified from plasmid pKT211. These PCR-generated fragments were used to transform yeast W303 strains followed by selection of either G418 resistance or histidine prototrophy.

Table A.1: Oligoucleotides used in strain construction.

Oligo	Sequence
1	GAATTCGGATCC**gtcgac**CCACATTGAACTTTTCACTTCG
2	GAATAATTCTTCACCTTTAGACATTTGGATTGTATTCGTGGAG
3	GAATTCGGATCC**gtcgac**ATTGAGTCGATGAGAGAGTG
4	GAATAATTCTTCACCTTTAGACATTTTGCCGCGTGGAGACATCTG
5	CTCCACGAATACAATCCAAATGTCTAAAGGTGAAGAATTATTC
6	CCTCCATGTCGCTGGCCGGGTGACCCGGCGGGGACGAGGC
7	CAGATGTCTCCACGCGGCAAAATGTCTAAAGGTGAAGAATTATTC
8	ttagcgattggcattatcacataatgaattatacattatataaagtaatgtgatttTTTACCGTTTAGTAGACAGAATGC
9	tagattggtatatatacgcatatgtggtgttgaagaaacatgaaattgcccagtatTTTACCGTTTAGTAGACAGAATGC
10	tttcttagcgattggcattatcacataatgaattatacattatataaagtaatgtgatttGTTTCCTACCCCAATGATG
11	gacttagattggtatatatacgcatatgtggtgttgaagaaacatgaaattgcccagtatGTTTCCTACCCCAATGATG
12	CCTTTGGTGGAGGGAACATCGTTGGTACCATTGGGCGAGGTGGCTTCTCTTATGGCAACCTCGATGAATTCGAGCTCG
13	TTTTGCTGGCCGCATCTTCTCAAATATGCTTCCCAGCCTGCTTTTCTGTAACGTTCACCCTCGATGAATTCGAGCTCG

Table A.2: Yeast Strains

Strain	Genotype
EY0105	*ade2-1 pho84::HIS3*
EY0329	*ade2-1 pho84::HIS3 pho4::TRP1*
EY1872	*spl2::CgLEU2*
EY1995	*MATa ura3::PPHO84-eGFP3-URA3*
EY2150	*MATa pho84::PPHO84-CFP-Kan PHO4-yECitrine-HIS3 spl2::CgLEU2 Nhp6a-mCherry-Nat*
EY2407	*HIS3::PPHO84-yECerulian-HIS3*
EY2408	*URA3::PPHO84-yECerulian-HIS3*
EY2409	*HIS3::PPHO84-yECitrine-HIS3*
EY2410	*URA3::PPHO84-yECitrine-HIS3*
EY2411	*HIS3::PSPL2-yECerulian-HIS3*
EY2412	*URA3::PSPL2-yECerulian-HIS3*
EY2413	*HIS3::PSPL2-yECitrine-HIS3*
EY2414	*URA3::PSPL2-yECitrine-HIS3*
EY2415	*HIS3::PPHO84-yECerulian-HIS3 URA3::PSPL2-yECitrine-HIS3*
EY2416	*HIS3::PPHO84-yECerulian-HIS3 URA3::PSPL2-yECitrine-HIS3 spl2::CgLEU2*
EY2417	*HIS3::PPHO84-yECerulian-HIS3 Nhp6a-mCherry-Nat PHO4-yECitrine-HIS3*
EY2418	*pho84::PPHO84-yECerulian-Kan spl2::PSpl2-yECitrine-HIS3*

All strains are derived from K699 *trp1-1 can1-100 leu2-3,112 his3-11,15 ura3*

SPL2 Annotation

Initial experiments utilizing *SPL2*-promoted fluorescent reporters showed no PHO-dependent induction of the reporters from the *SPL2* promoter. This was in contrast to previous microarray experiments that showed large increases in *SPL2* expression upon phosphate starvation (Ogawa et al., 2000). Additionally, when overexpressed by a heterologous promoter, Spl2 migrated at a larger size than native Spl2 (Wykoff et al., 2007). Analysis of the *SPL2* sequence indicated two in-frame ATG codons downstream of the published *SPL2* initiating codon (Flick and Thorner, 1998). This led us to suspect that the published *SPL2* sequence was incorrectly annotated, with translation initiating from one of the two downstream codons.

To aid in identification of the actual *SPL2* initiating ATG, the *SPL2* sequence was aligned using ClustalW to the *SPL2* sequences of related fungi. In comparisons of fungal orthologs, it is common to see relatively high levels of homology in coding regions. In promoter regions, on the other hand, relatively low levels of homology are interspersed with short regions of high homology that typically correspond to protein binding sites in the promoter (Cliften et al., 2003; Kellis et al., 2003). In the region between the published initiating ATG and the most downstream ATG, the alignments showed relatively low homology between the orthologs, with a single

short segment of higher homology reminiscent of a TATA box. Beginning with downstream ATG, levels of homology between the orthologs rise (Figure A.1). This suggested to us that the downstream ATG was the real initiating codon. If this is true, constructs utilizing the presumptive *SPL2* promoter to drive heterologous proteins would likely be non-functional as approximately 100 base pairs of the actual promoter (potentially including a TATA box) would have been missing in these constructs.

Therefore, new *SPL2* promoter constructs were built that utilized a promoter fragment that extended up to the 2nd downstream ATG. When transformed into yeast, these new constructs showed marked reporter induction upon phosphate starvation. Additonally, when overexpressed by a heterologous promoter, Spl2 migrates at the same size as native Spl2 when utilizing the 2nd downstream ATG as the initiating codon (Wykoff et al., 2007).

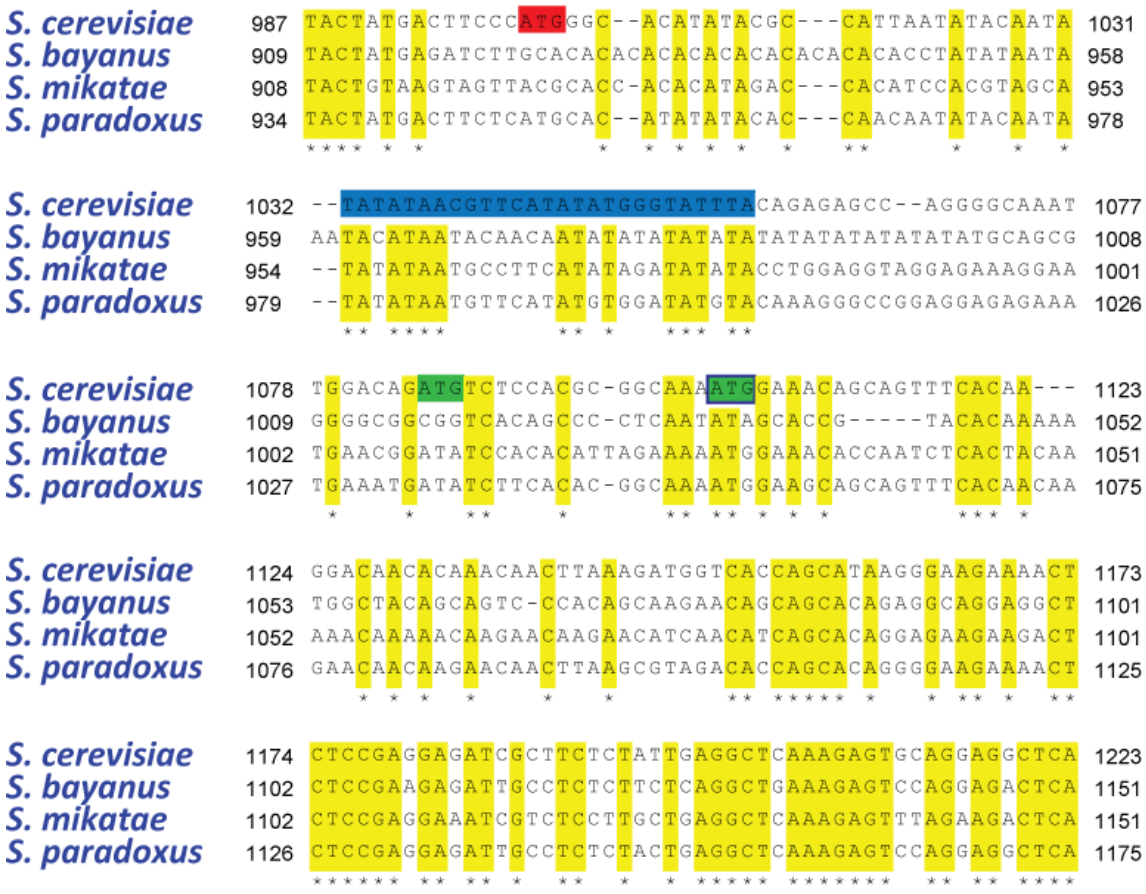

Figure A.1: Sequence alignment of *SPL2* and orthologs.

The *S. cerevisiae SPL2* sequence and its orthologs from *S. bayanus, S. mikatae, and S. paradoxus* were aligned using the ClustalW algorithm. Identical nucleotides are highlighted in yellow. The published initiating codon is highlighted in red. The two downstream in frame ATG codons are highlighted in green. The presumptive initiating ATG codon, which was used for all experiments, is highlighted in green with blue outline. A putative TATA box is highlighted in blue.

Matlab Code

New2dbif. 2-dimensional bifurcation analysis of the PHO model.

```
function finali=new2dbif()

%% Variable Definition
syms E p Th Tl
vl = 0.0038197; kl = 250e-6; vh = 0.00305577; kh = 9e-6; bh = .00693;
bl =.00693; nl = 6; nh = 6; g = .00693;
pend=(E*((bh*vh)/((E + kh)*(1 + (p/Th)^nh)) + (bl*vl)/((E + kl)*(1 +
(Tl/p)^nl)))) / g - g*p;
dpend=diff(pend,'p');

%% Parameters

TlTl=linspace(.03,.2,25);
ThTh=linspace(.03,.2,25);

%% Initialize Output Variables
finali=[];
abort=false;
h=awaitbar(0,'running...');

%% Main Loop

for i=1:length(TlTl)
    Tl=TlTl(i);
    finall=[];

    for l=1:length(ThTh)
        Th=ThTh(l);
        S=solve(subs(pend),subs(dpend));
        results=double([S.p,S.E]);
        rp(:,1)=realpos(results(:,1));
        rp(:,2)=realpos(results(:,2));
        rp(:,3)=Tl;
        rp(:,4)=Th;
        finall=[finall;rp];
        results=[];
        rp=[];
        if abort; close(h); break; end   % Abort the loop by clicking
abort button
```

```
        if isempty(h); break; end     % Break the loop when closing the
figure
    end

    if abort; close(h); break; end   % Abort the loop by clicking abort
button
    if isempty(h); break; end     % Break the loop when closing the
figure
    finali=[finali;finall];
    h=awaitbar(i/length(TlTl),h,'running...','Progress');
end




surf(E,Tl,prs);
shading interp;
view(2);
hold on;

full=xlsread('C:\Users\Brian\Desktop\full.xls');
plot3(full(1:20,1),full(1:20,2),full(1:20,4),'-k','LineWidth',4);
plot3(full(21:end,1),full(21:end,2),full(21:end,4),'-k','LineWidth',4);

hold off;

axis tight;
```

histfilesB: Loads a directory of flow cytometry data files, finds phosphate concentrations and fluorescence channels and passes data to gating and/or plotting functions.

```
%     Copyright 2007 Brian Margolin & Felix Lam
%     brian.margolin@ucsf.edu

%     This program is free software; you can redistribute it and/or
modify
%     it under the terms of the GNU General Public License as published
by
%     the Free Software Foundation; either version 3 of the License, or
%     (at your option) any later version.
%
%     This program is distributed in the hope that it will be useful,
%     but WITHOUT ANY WARRANTY; without even the implied warranty of
%     MERCHANTABILITY or FITNESS FOR A PARTICULAR PURPOSE.  See the
%     GNU General Public License for more details.
%
%     You should have received a copy of the GNU General Public License
%     along with this program.  If not, see
<http://www.gnu.org/licenses/>.


%   histfilesB(PATTERN) - plots a series of histograms of the .fcs
files in the current
%   directory.  Supply a string PATTERN to restrict to a subset of
files.  The .fcs
%   extension is automatically added.  If you leave PATTERN blank, all
the .fcs
%   files in the current directory will be read.
%
%   Examples:
%
%   HISTFILES
%   HISTFILES('1907')
%   HISTFILES('1907*mM')
%
%Brian Margolin based on original code by F. Lam - 6/2006

function [data, concs]=histfilesB(varargin)

if isempty(varargin)
    pattern = '';
    gate=1;
```

```
end

if nargin==1;
    if ischar(varargin{:})
        pattern = ['*' char(varargin)];
    elseif isnumeric(varargin{:})
        pattern = '';
        gate=varargin{1};
    end
end

if nargin==2;
    if ischar(varargin{1})
        pattern = ['*' char(varargin(1))];
        gate=varargin{2};
    else gate=varargin{1};
        pattern = ['*' char(varargin(2))];
    end
end

% ------------------------------------ MAIN LOOP --------------------
---------------
dirname=uigetdir('%HOMEPATH%\Desktop','Choose a Directory');
d = dir([dirname '/' pattern '*.fcs']);
numfile = length(d);
concs=zeros(1,numfile);

if numfile == 0
    error('No files match pattern.');
end

[fcsdata, header]   = fca_readfcs([dirname '/' d(1).name]);

for i=1:length(header.par)
    temp{1,i}=header.par(i).name;
end
paramlist=temp;
k=menu('Select Parameter to Plot',temp);
match=paramlist(k);
data = cell(1, numfile);
position=[];

columns=4;
rows=ceil(numfile/4);


for i = 1:numfile
    position = findstr(d(i).name,'_');
    if isempty(position)
```

```
    temp=[];
    temp=d(i).name;
    temp=strrep(temp, '.fcs', '');
    temp=strrep(temp, '-', '.');
    temp2=isletter(temp);
    temp(temp2)=[];
    concs(1,i)=str2num(temp);
elseif position==1;
    temp=[];
    temp=d(i).name;
    temp=strrep(temp, '.fcs', '');
    temp=strrep(temp, '-', '.');
    temp=strrep(temp, '_', '');
    temp2=isletter(temp);
    temp(temp2)=[];
    concs(1,i)=str2num(temp);
else
    temp=[];
    position=position(end);
    temp=d(i).name;
    temp(1:position)=[];
    temp=strrep(temp, '.fcs', '');
    temp=strrep(temp, '-', '.');
    temp2=isletter(temp);
    temp(temp2)=[];
    concs(1,i)=str2num(temp);
end
    [fcsdata, header]   = fca_readfcs([dirname '/' d(i).name]);

% Look in header to find first column which is FITC
for j = 1:length(header.par)
    if strmatch(match, header.par(j).name)
        gfpcol = j;
        break
    end
end

% Look in header to find FSC-A & SSC-A for gating.
for j = 1:length(header.par)
    if strmatch('FSC-A', header.par(j).name)
        fsc = j;
        break
    end
end
for j=1:length(header.par)
    if strmatch('SSC-A', header.par(j).name)
        ssc=j;
        break
    end
end
```

```
    [r,c]=find(2e5<fcsdata(:,gfpcol) | fcsdata(:,gfpcol)<10);
    fcsdata(r,:)=[];
    [r,c]=find(2e5<fcsdata(:,fsc) | fcsdata(:,fsc)<10000);
    fcsdata(r,:)=[];
    [r,c]=find(2e5<fcsdata(:,ssc) | fcsdata(:,ssc)<10000);
    fcsdata(r,:)=[];

    if gate==1

ix=dscatterB(fcsdata(:,fsc),fcsdata(:,ssc),'plottype','contour');

dataix=inpolygon(fcsdata(:,fsc),fcsdata(:,ssc),ix(:,1),ix(:,2));
        datagated=[];
        for p = 1: length (fcsdata)
            if dataix(p)==1
                datagated = [datagated;fcsdata(p,:)];
            end
        end
        fldata=datagated(:,gfpcol);
        if (~exist([dirname, '\gates\'],'dir'))
            mkdir(dirname, 'gates');
        else
        end
        save([dirname, '\gates\', num2str(concs(i)),'.mat'], 'ix');

    elseif gate==2
        load ([dirname, '\gates\', num2str(concs(i)),'.mat']);

dataix=inpolygon(fcsdata(:,fsc),fcsdata(:,ssc),ix(:,1),ix(:,2));
        datagated=[];
        for p = 1: length (fcsdata)
            if dataix(p)==1
                datagated = [datagated;fcsdata(p,:)];
            end
        end
        fldata=datagated(:,gfpcol);

    else
        fldata=fcsdata(:,gfpcol);
    end

    % Eliminate negative data points (b/c of log scale)
    %     gate  = find(fcsdata(:,gfpcol) > 0);

    if gate==1
        figure(1);
        subplot(rows,columns,i),
```

```
        dscatter(fcsdata(:,1),fcsdata(:,3));
        lbl=[num2str(concs(i)) ' '  texlabel('mu') 'M'];
        text(.5e5,.1e5,lbl);
        hold on;
        if gate ~= 0
            plot(ix(:,1),ix(:,2),'-r');
        end
        hold off;
    end



    data{i}=fldata;
    disp([num2str(concs(i)) ' - ' num2str(median(data{i}))]);
end


denseriesB([min(cellfun(@min, data)), max(cellfun(@max, data))], concs,
data{1:end});

k=menu('Do you want to save the data to an Excel file?','Yes', 'No');

if k==1
    pad=max(cellfun(@length,data));
    datapad=zeros(pad,numfile);
    for i=1:numfile
        padsize=pad-(length(data{i}));
        datapad(:,i)=padarray(data{i},padsize,'post');
    end

    [file,path] = uiputfile('*.csv','Save Workspace As');
    %   col=char('A'+(i-1));
    %   xlswrite([path,file],data{i},'Sheet1', [col, '1']);
    csvwrite([path,file],datapad);

else
end
```

dscatterB: Uses forward and side scatter data to make contour plots of flow cytometry data. Uses the contour data to identify population of single cells. Discards cell clumps and debris and hands back to initiating function.

```
function ix = dscatterB(X,Y, varargin)


lambda      = [];
nbins       = [];
plottype    = 'scatter';
contourFlag = false;
msize       = 2;
marker      = 'o';
logy        = false;
filled      = true;

if nargin > 2
    if rem(nargin,2) == 1
        error('Bioinfo:IncorrectNumberOfArguments',...
            'Incorrect number of arguments to %s.',mfilename);
    end
    okargs =
{'smoothing','bins','plottype','logy','marker','msize','filled'};
    for j=1:2:nargin-2
        pname = varargin{j};
        pval = varargin{j+1};
        k = strmatch(lower(pname), okargs); %#ok
        if isempty(k)
            error('Bioinfo:UnknownParameterName',...
                'Unknown parameter name: %s.',pname);
        elseif length(k)>1
            error('Bioinfo:AmbiguousParameterName',...
                'Ambiguous parameter name: %s.',pname);
        else
            switch(k)
                case 1  % smoothing factor
                    if isnumeric(pval)
                        lambda = pval;
                    else
                        error('Bioinfo:InvalidScoringMatrix','Invalid
smoothing parameter.');
                    end
                case 2
                    if isscalar(pval)
                        nbins = [ pval pval];
```

```
                    else
                        nbins = pval;
                    end
                case 3
                    plottype = pval;
                case 4
                    logy = pval;
                    Y = log10(Y);
                case 5
                    contourFlag = pval;
                case 6
                    marker = pval;
                case 7
                    msize = pval;
                case 8
                    filled = pval;
            end
        end
    end
end

%Remove small points likely to be debris.
x=find(X<.2e5);
X(x)=[];
Y(x)=[];
y=find(Y<.15e5);
X(y)=[];
Y(y)=[];



minx = min(X,[],1);
maxx = max(X,[],1);
miny = min(Y,[],1);
maxy = max(Y,[],1);

if isempty(nbins)
    nbins = [min(numel(unique(X)),200) ,min(numel(unique(Y)),200) ];
end

if isempty(lambda)
    lambda = 10;
end

edges1  = linspace(minx, maxx, nbins(1)+1);
ctrs1   = edges1(1:end-1) + .5*diff(edges1);
edges1  = [-Inf edges1(2:end-1) Inf];
edges2  = linspace(miny, maxy, nbins(2)+1);
ctrs2   = edges2(1:end-1) + .5*diff(edges2);
```

```
edges2  = [-Inf edges2(2:end-1) Inf];

[n,p]   = size(X);
bin     = zeros(n,2);

% Reverse the columns to put the first column of X along the horizontal
% axis, the second along the vertical.
[dum,bin(:,2)] = histc(X,edges1);
[dum,bin(:,1)] = histc(Y,edges2);
H = accumarray(bin, 1, nbins([2 1])) ./ n;
G = smooth1D(H, nbins(2)/lambda);
F = smooth1D(G', nbins(1)/lambda)';
% = filter2D(H,lambda);

if logy
    ctrs2 = 10.^ctrs2;
    Y = 10.^Y;
end

okTypes = {'surf','mesh','contour','image','scatter'};
k = strmatch(lower(plottype), okTypes); %#ok

if isempty(k)
    error('dscatter:UnknownPlotType',...
        'Unknown plot type: %s.',plottype);
elseif length(k)>1
    error('dscatter:AmbiguousPlotType',...
        'Ambiguous plot type: %s.',plottype);

else
    switch(k)

        case 1 %'surf'
            h = surf(ctrs1,ctrs2,F,'edgealpha',0);
        case 2 % 'mesh'
            h = mesh(ctrs1,ctrs2,F);
        case 3 %'contour'
            h=figure('visible','off');
            [c, h] =contour(ctrs1,ctrs2,F,15);
            v=get(h,'LevelList');
            xcg=get(get(h,'children'),'xdata');
            ycg=get(get(h,'children'),'ydata');
            ix=getconB;
        case 4 %'image'
            nc = 256;
            F = F./max(F(:));
            colormap(repmat(linspace(1,0,nc)',1,3));
            h =image(ctrs1,ctrs2,floor(nc.*F) + 1);
        case 5 %'scatter'
```

```
            F = F./max(F(:));
            ind = sub2ind(size(F),bin(:,1),bin(:,2));
            col = F(ind);
            if filled
                h = scatter(X,Y,msize,col,'ko','filled');
            else
                h = scatter(X,Y,msize,col,'ko',marker);
            end
    end
    f=gcf;
    close(f);
end

if logy
    set(gca,'yscale','log');
end


    function ix=getconB

        if length(v) == 1
            oneslice = 1;
            v = [v v];
        else
            oneslice = 0;
            if length(unique(v)) ~= length(v)
                error('Contour slice altitudes must be unique')
            end
        end

        if oneslice
            if iscell(xcg)
                xc=cat(1,xcg{:});
                yc=cat(1,ycg{:});
            else
                xc=xcg;
                yc=ycg;
            end
        else % multiple slices; return cell array
            sa = get(get(h,'children'),'userdata'); % slice altitudes
            if iscell(sa) % if only one slice is nonempty, sa will be
scalar
                sa = [sa{:}];
            end
            %if length(sa)
            % preallocate cell array space
            xc{length(v)}=[];
            yc{length(v)}=[];
            for n = 1:length(v) % loop through slice altitudes
                k = sa==v(n);
```

```
    if any(k)
        if iscell(xcg)
            xc{n}=cat(1,xcg{k});
            yc{n}=cat(1,ycg{k});
        else % non-cell when only one non-empty slice
            xc{n}=xcg(:);
            yc{n}=ycg(:);
        end
        xn=find(~(xc{n}>0),1);
        xc{n}(xn:end)=[];
        yc{n}(xn:end)=[];

    end
end
temp=axis;
i=1;
while i<length(xc)
    if find (xc{i}==temp(1))

        xc(i)=[];
        yc(i)=[];
    else
        i=i+1;
    end
end
i=1;
while i<length(xc)
    if find (xc{i}==temp(2))

        xc(i)=[];
        yc(i)=[];
    else
        i=i+1;
    end
end
i=1;
while i<length(xc)
    if find (yc{i}==temp(3))

        xc(i)=[];
        yc(i)=[];
    else
        i=i+1;
    end
end
i=1;
while i<length(xc)
    if find (yc{i}==temp(4))
        xc(i)=[];
        yc(i)=[];
```

```
            else
                i=i+1;
            end
        end

        areas=zeros(length(xc),1);
        for q=1:length(xc)
            areas(q)=polyarea(xc{q},yc{q});
        end


        i=1;
        while i<length(areas)
            if areas(i) < .001e9
                areas(i) = [];
                xc(i)=[];
                yc(i)=[];
            else
                i=i+1;
            end
        end


        [N,IX]=sort(areas);
        xc=xc(IX);
        yc=yc(IX);

        dens=zeros(length(xc),1);
        for i=1:length(xc)

dens(i)=(numel(X(inpolygon(X,Y,xc{i},yc{i}))))/(polyarea(xc{i},yc{i}));
        end

        [N,IX]=sort(dens,'descend');
        xc=xc(IX);
        yc=yc(IX);


        cen1=centroid(length(xc{1}),[xc{1},yc{1}]');
        i=1;
        while i < (length(xc)+1)

            testcen = centroid(length(xc{i}),[xc{i},yc{i}]');
            distance=sqrt((testcen(2)-cen1(2))^2 + (testcen(1)-
cen1(1))^2);

            if distance > 5000
                xc(i)=[];
```

```
                yc(i)=[];
            else
                i=i+1;
            end

        end

        areas=zeros(length(xc),1);
        for o=1:length(xc)
            areas(o)=polyarea(xc{o},yc{o});
        end
        [N,IX]=sort(areas,'descend');
        xc=xc(IX);
        yc=yc(IX);
        ix=[xc{1},yc{1}];


    end
  end
end

function Z = smooth1D(Y,lambda)
[m,n] = size(Y);
E = eye(m);
D1 = diff(E,1);
D2 = diff(D1,1);
P = lambda.^2 .* D2'*D2 + 2.*lambda .* D1'*D1;
Z = (E + P) \ Y;
end
```

denseriesB: Takes gated flow cytometry data and plots as a density map using phosphate concentrations on the x-axis.

```
function denseriesB(ylims, concs, varargin)


numseries   = length(varargin);

% Parameters for histogram binning, and interpolation (smoothed) points
histbins    = 20;
interpbins  = 20;
dist=length(concs)-1;
for i=1:(length(concs)-1)
    dist(i)=abs(concs(i)-concs(i+1));
end
spread = (min(dist)/2).*1e-6;

[xcenters,IX] = sort(concs);
xcenters=xcenters.*1e-6;
datasorted=varargin(IX);

xspread=zeros(1,4*numseries);
xspread(3:4:end)=xcenters - spread;
xspread(4:4:end)=xcenters + spread;

for i=5:4:length(xspread)
    xspread(i)=xspread(i-1);
    xspread(i+1)=xspread(i+2);
end
xspread(2)=xspread(3);
binstmp     = logspace(log10(ylims(1)), log10(ylims(2)), histbins)';
bins        = logspace(log10(ylims(1)), log10(ylims(2)), interpbins)';
Z           = zeros(interpbins, length(xspread));

for i = 1:numseries
    tmp = hist(datasorted{i}, binstmp)';

    % Smooth by interpolation
    %y  = interp1(binstmp, tmp, bins, 'pchip');
    y=tmp;
    % Normalize histograms
    Z(:,i*4) = y / sum(y);
    Z(:,i*4-1) = Z(:,i*4);
    ZZ(i,:)=y / max(y);
end
```

```
%bins=bins ./ 1.1e4;
figure;
surf((xspread), bins, Z); shading interp;
set(gca, 'yscale', 'log');
axis tight;
view(2);


% Create xlabel
xlabel('\bf{P_{i} (M)}');

% Create ylabel
ylabel('\bf{Fluorescence (a.u.)}');
```

References

Amberg, D.C., D. Botstein, and E.M. Beasley. 1995. Precise gene disruption in Saccharomyces cerevisiae by double fusion polymerase chain reaction. *Yeast*. 11:1275-80.

Angeli, D., J.E. Ferrell, Jr., and E.D. Sontag. 2004. Detection of multistability, bifurcations, and hysteresis in a large class of biological positive-feedback systems. *Proc Natl Acad Sci U S A*. 101:1822-7.

Bar-Even, A., J. Paulsson, N. Maheshri, M. Carmi, E. O'Shea, Y. Pilpel, and N. Barkai. 2006. Noise in protein expression scales with natural protein abundance. *Nat Genet*. 38:636-43.

Barkai, N., and S. Leibler. 1997. Robustness in simple biochemical networks. *Nature*. 387:913-7.

Bun-Ya, M., M. Nishimura, S. Harashima, and Y. Oshima. 1991. The PHO84 gene of Saccharomyces cerevisiae encodes an inorganic phosphate transporter. *Mol Cell Biol*. 11:3229-38.

Campbell, R.E., O. Tour, A.E. Palmer, P.A. Steinbach, G.S. Baird, D.A. Zacharias, and R.Y. Tsien. 2002. A monomeric red fluorescent protein. *Proc Natl Acad Sci U S A*. 99:7877-82.

Carroll, A.S., A.C. Bishop, J.L. DeRisi, K.M. Shokat, and E.K. O'Shea. 2001. Chemical inhibition of the Pho85 cyclin-dependent kinase reveals a role in the environmental stress response. *Proc Natl Acad Sci U S A*. 98:12578-83.

Cliften, P., P. Sudarsanam, A. Desikan, L. Fulton, B. Fulton, J. Majors, R. Waterston, B.A. Cohen, and M. Johnston. 2003. Finding functional features in Saccharomyces genomes by phylogenetic footprinting. *Science*. 301:71-6.

Cormack, B.P., R.H. Valdivia, and S. Falkow. 1996. FACS-optimized mutants of the green fluorescent protein (GFP). *Gene*. 173:33-8.

Deacon, J.W. 2006. Fungal biology. Blackwell Pub., Malden, MA. 371 p. pp.

Ferrell, J.E., Jr., and E.M. Machleder. 1998. The biochemical basis of an all-or-none cell fate switch in Xenopus oocytes. *Science*. 280:895-8.

Flick, J.S., and J. Thorner. 1998. An essential function of a phosphoinositide-specific phospholipase C is relieved by inhibition of a cyclin-dependent protein kinase in the yeast Saccharomyces cerevisiae. *Genetics*. 148:33-47.

Griesbeck, O., G.S. Baird, R.E. Campbell, D.A. Zacharias, and R.Y. Tsien. 2001. Reducing the environmental sensitivity of yellow fluorescent protein. Mechanism and applications. *J Biol Chem*. 276:29188-94.

Hartwell, L.H., J.J. Hopfield, S. Leibler, and A.W. Murray. 1999. From molecular to modular cell biology. *Nature*. 402:C47-52.

Kellis, M., N. Patterson, M. Endrizzi, B. Birren, and E.S. Lander. 2003. Sequencing and comparison of yeast species to identify genes and regulatory elements. *Nature*. 423:241-54.

Kitada, K., E. Yamaguchi, and M. Arisawa. 1995. Cloning of the Candida glabrata TRP1 and HIS3 genes, and construction of their disruptant strains by sequential integrative transformation. *Gene*. 165:203-6.

Kremers, G.J., J. Goedhart, E.B. van Munster, and T.W. Gadella, Jr. 2006. Cyan and yellow super fluorescent proteins with improved brightness, protein folding, and FRET Forster radius. *Biochemistry*. 45:6570-80.

Longtine, M.S., A. McKenzie, 3rd, D.J. Demarini, N.G. Shah, A. Wach, A. Brachat, P. Philippsen, and J.R. Pringle. 1998. Additional modules for versatile and economical PCR-based gene deletion and modification in Saccharomyces cerevisiae. *Yeast*. 14:953-61.

Maerkl, S.J., and S.R. Quake. 2007. A systems approach to measuring the binding energy landscapes of transcription factors. *Science*. 315:233-7.

Maheshri, N., and E.K. O'Shea. 2007. Living with noisy genes: how cells function reliably with inherent variability in gene expression. *Annu Rev Biophys Biomol Struct*. 36:413-34.

Newman, J.R., S. Ghaemmaghami, J. Ihmels, D.K. Breslow, M. Noble, J.L. DeRisi, and J.S. Weissman. 2006. Single-cell proteomic analysis of S. cerevisiae reveals the architecture of biological noise. *Nature*. 441:840-6.

O'Neill, E.M., A. Kaffman, E.R. Jolly, and E.K. O'Shea. 1996. Regulation of PHO4 nuclear localization by the PHO80-PHO85 cyclin-CDK complex. *Science*. 271:209-12.

Ogawa, N., J. DeRisi, and P.O. Brown. 2000. New components of a system for phosphate accumulation and polyphosphate metabolism in Saccharomyces cerevisiae revealed by genomic expression analysis. *Mol Biol Cell*. 11:4309-21.

Sheff, M.A., and K.S. Thorn. 2004. Optimized cassettes for fluorescent protein tagging in Saccharomyces cerevisiae. *Yeast*. 21:661-70.

Sikorski, R.S., and P. Hieter. 1989. A system of shuttle vectors and yeast host strains designed for efficient manipulation of DNA in Saccharomyces cerevisiae. *Genetics*. 122:19-27.

Springer, M., D.D. Wykoff, N. Miller, and E.K. O'Shea. 2003. Partially phosphorylated Pho4 activates transcription of a subset of phosphate-responsive genes. *PLoS Biol*. 1:E28.

Thomas, M.R., and E.K. O'Shea. 2005. An intracellular phosphate buffer filters transient fluctuations in extracellular phosphate levels. *Proc Natl Acad Sci U S A*. 102:9565-70.

Vogel, K., W. Horz, and A. Hinnen. 1989. The two positively acting regulatory proteins PHO2 and PHO4 physically interact with PHO5 upstream activation regions. *Mol Cell Biol*. 9:2050-7.

Wykoff, D.D., and E.K. O'Shea. 2001. Phosphate transport and sensing in Saccharomyces cerevisiae. *Genetics*. 159:1491-9.

Wykoff, D.D., A.H. Rizvi, J.M. Raser, B. Margolin, and E.K. O'Shea. 2007. Positive feedback regulates switching of phosphate transporters in S. cerevisiae. *Mol Cell*. 27:1005-13.

Publishing Agreement

It is the policy of the University to encourage the distribution of all theses and dissertations. Copies of all UCSF theses and dissertations will be routed to the library via the Graduate Division. The library will make all theses and dissertations accessible to the public and will preserve these to the best of their abilities, in perpetuity.

Please sign the following statement:

I hereby grant permission to the Graduate Division of the University of California, San Francisco to release copies of my thesis or dissertation to the Campus Library to provide access and preservation, in whole or in part, in perpetuity.

Author Signature